Examensarbete
TVVR 13/5002

# Analysis of Trends and Patterns of Droughts Using Satellite Data and Climate Model Simulations

Lisa Damberg


Division of Water Resources Engineering
Department of Building and Environmental Technology

Avd för Teknisk Vattenresurslära
TVVR-YY/500n
ISSN 1101-9824

# Analysis of Trends and Patterns of Droughts Using Satellite Data and Climate Model Simulations

Lisa Damberg

# Analysis of Trends and Patterns of Droughts Using Satellite Data and Climate Model Simulations

Lisa Damberg

**Abstract**

Numerous studies indicate that the frequency of extreme events such as droughts have increased particularly in the 20th century. Droughts are considered among the most costly natural disasters due to their impacts on crop yield, infrastructure, industry, and tourism. This thesis investigates historical global trends and patterns of droughts and drying areas. A satellite-based (model independent) climate data record is used along with historical information from the latest CMIP5 multi-model simulations. For the CMIP5 simulations the objective include a comparison with validated ground observations.

The focus is on meteorological droughts, defined as a lack of precipitation, and the Standardized Precipitation Index (SPI) is used to analyze fractions of area under drought (SPI $\leq$ -1) and area experiencing extreme droughts (SPI $\leq$ -2) at a quasi-global scale, for the length of the records available. From the 32-year long record, based on merged satellite product from GPCP and PERSIANN data, and from the CMIP5 simulations between 1901 -2005, the results show similar pattern for the Southern Hemisphere (SH) where variability is larger than in the Northern Hemisphere (NH).

When investigating trends of land area in drought, only the SH show a significant trend using Mann-Kendall's test on the merged satellite based product. However, over oceans drought areas indicate an increase, for both hemispheres and the globe as a total. When studying the CMIP5 simulations and comparing them to ground observations 73% of the models recapture the trends in the observations, for the global land area, as well as for the NH and the SH, separately. Both datasets indicate larger variability of area in drought for the SH than for the NH, for extreme as well as more moderate droughts.

From the analysis of spatial patterns of wetting and drying trends maps were created from the pixel-based satellite data and several regions, such as the southwestern United States, Texas, parts of the Amazon, the Horn of Africa, and northern India exhibit a drying trend. The results from the CMIP5 models were generally consistent with observations at a global (semi-global) scale, but most models were not in agreement with observations with respect to regional drying and wetting trends. However, CMIP5 simulations of regional trends are collectively in better agreement with observations over high latitudes, as well as northeastern India and the western United States.

# Acknowledgements

First of all I would like to express my gratitude to my mentor and advisor: Professor Amir AghaKouchak of the Hydroclimate Research Group at University of California, Irvine, who not only gave me the opportunity to work on this fascinating material and assisted with all administration included in preparing ones Master thesis abroad but also provided encouragement at all times.
Thank you.

I also wish to thank Cintia B.-Uvo, (Lund University,Department of Civil Engineering), for taking the time to be my examinator.

I would also like to thank my coworkers in the Hydroclimate Research Group; Zengchao Hao for invaluable advise and explanations on all subjects possible, badminton not the least; Navid Nakhjiri; for help with my codes, and with foreign languages of all kinds; Linyin Cheng, Ali Mehran and Alireza Farahmand; for discussions, support and all the fun.

I am also thankful to my friends and family in Sweden, who supported my extended stay in California to work on this thesis. Especially Gustav. To all wonderful Californian friends, and my almost-family the Collins' ; thanks for all the help and and support out here. UCI Women's Rowing team made sure I woke up on time every morning, and they will always have my gratitude for that, and more.

With regard to the research and materials included in this thesis we are most grateful for the considerable amount of work of processing the data used. Especially a big thanks to Professor Thomas Phillips of the National Livermore National Lab for providing remapped information from the CMIP5 simulations.

We acknowledge the World Climate Research Programme's Working Group on Coupled Modelling, which is responsible for CMIP, and we thank the climate-modeling groups for producing and making available their model output. For CMIP, the U.S. Department of Energy's Program for Climate Model Diagnosis and Intercomparison provides coordinating support and leads the development of software infrastructure in partnership with the Global Organization for Earth System Science Portals.

# Sammanfattning

Torka är en naturkatastrof som globalt anses vara en av de mest kostsamma, då den påverkar såväl matproduktion, industrier, vildliv och inte minst tursim. Forskningen tyder även på ökad frekvens och utbredning av områden under torka under det senaste århundradet (Dai, 2012), (Frich et al., 2002). Syftet med uppsatsen är att undersöka mönster och trender för områden i torka på en semi-global skala med hjälp av ett satellitbaserad nederbördsinformation från 1979-2012 (sammanfogad data från produkterna GPCP och PERSIANN) och med simulerad nederbördsdata från CMIP5 modeller. Vad gäller modelldata, täcker nederbördsinformationen hela senaste århundradet, och totalt har 41 fristående simulaeringar från modelleringscentra över hela världen analyserats med hänsyn till hur väl de replikerar markobservationer från Climate Research Unit (CRU).

I studien defineras torka som brist på nederbörd med hjälp av "Standardized Precipitation Index" (SPI, (McKee et al., 1993) ) och dess tröskelvärde för torka ( SPI $\leq$ -1 ) och extrem torka (SPI $\leq$ -2). Enligt den satellitbaserade dataserien är i genomsnitt 15-16% av jorden under torka varav 2-3 % definerades uppleva extrem torka. De modellbaserade resultaten visar ett medelvärde på ca 15-16% i torka, vilket stämmer väl med observerade CRU resultat.

Trender för area under torra förhållanden undersöks med Mann-Kendall's test, och för de satellitbaserade resultaten upptäcks en signifikant trend för total area och över oceanerna. Över land kan ingen sådan trend observeras förrän Norra och Södra hemisfärerna studeras separat då södra halvklotet uppvisar en trend på signifkansnivån p=0.05. Resultaten baserade på simulerad nederbörd visar trender som stämmer överens med observerade trender både globalt, och för norra och södra halvkloten separat i 73% av de analyserade modellerna. Vidare kan en större variabilitet för area i torka noteras för södra halvklotet i jämförelse med norra halvklotet.

Slutligen analyserades den rumsliga utbredningen av torrare/blötare trender genom att, för varje pixel, applicera Mann-Kendalls test över tid och konstatera en ökning eller minskning av SPI. Från den satellitbaserade undersökningen visar flera områden som upplevt torkor nyligen en trend av uttorkning över tid, exempelvis sydvästra USA, Texas, delar av Amazonas, Afrikas horn och norra Indien. Överensstämmelsen mellan CMIP5 simuleringar och observationer är överlag bättre pN̆ högre latituder, och trots att trenderna för torka globalt sett återskapas av flertalet modeller är de regionala överensstämmelserna lägre, omkring 40% i genomsnitt.

# Table of Contents

# Abbreviations

| | |
|---|---|
| ANN | Artificial Neural Network |
| AOGCM | AtmosphereOcean Global Climate Models |
| CHRS | Center for Hydrometerology and Remote Sensing |
| CMIP5 | Climate Modeling Intercomparison Project Phase 5 |
| CMORPH | CPC Morhing technique |
| CRU | Climate Research Unit |
| EMIC | Earth system Model of Intermediate Complecity |
| EMS | Earth System Model |
| ENSO | El Nino Southern Oscillation |
| EOS | eart Orbiting Satellites |
| GEWEX | Global Energy and Water Experiment |
| GPCP | Global Precipiation Climatology Project |
| GSFC | Goddard Space and Flight Center |
| IPCC | Intergovernal Panel on Climate Change |
| IPO | Inderdecadal Pacific Oscillation |
| MK | Mann-Kendall |
| NASA | National Aeronautics and Space Administration |
| NDVI | Normalized Difference Vegetation Index |
| NDWI | Normalized Differnce Water Index |
| NH | Northern Hemisphere |
| NOAA | National Oscenic and Atmospheric Administraion |
| PDSI | Palmer's Drought Severity Index |
| PERSIANN | Precipitation Estimation from Remotely Sensed Information using Articial Neural Networks |
| PHDI | Palmer's Hydrological Drought Index |
| POD | Probability Of Detection |
| SH | the Southern Hemisphere |
| SMI | Soil Moisture Index |
| SPEI | Standardized Precipitaion Evaporation Index |
| SPI | Standardized Precipitation Index |
| SRI | Standardized Runoff Index |
| SWEI | Surface Water Supply Index |
| TMPA | TRMM Multisatellite Precipitation Analysis |
| TRMM | Tropical Rainfall Measuring Mission |
| VCI | Vegetation Cover Index |
| VegDRI | Vegetation Drought Response Index |
| WCRP | World Climate Research Project |
| WGCM | Working Group on Coupled Modeling |
| WMO | World Meterological Organization |

# Figures

# Tables

# 1 Introduction

This thesis is presented as the conclusion of my studies at the program of Civil Engineering at the Technical Faculty of Lund University and was performed at the Hydroclimate Research Group at University of California, Irvine. The focus of the thesis shifted slightly as the group got access to data of the CMIP5 simulations, thanks to Thomas Phillips at Lawrence Livermore National Laboratory. I have chosen to only present completed work in the thesis, and mention work in process in the Chapter 6.3.

## 1.1 Background and Motivation

Numerous studies indicate that the frequency of extreme events such as droughts have increased particularly in the 20th century (Dai, 2012), (Frich et al., 2002). Major drought events have been reported in the United States, Horn of Africa, Australia, and southern Europe in the past few decades. Texas, for example, experienced two record droughts in 2011 and 2006 resulting in billions of dollars in economic losses (AghaKouchak et al., 2012). In Hayes (2012) the droughts of the United States are claimed to be responsible for 25% of all weather related losses, at a total more than of $180 billions between 1980 and 2010. Droughts are considered among the most costly natural disasters due to their impacts on crop yield, infrastructure, industry, and tourism Wilhite (2000). Large economical impact, drought related famines and increased risk for forest fires, especially in drought vulnerable regions, show the importance of drought monitoring. Numerous model-based studies indicate that droughts and dry spells have become (or may become) more severe and/or more frequent in the future (Wehner, 2012) (Dai, 2011). This thesis investigates historical global trends and patterns of droughts and drying areas using a satellite-based (model independent) climate data record and information of CMIP5 multi-model and ground observations.

Most studies of historical droughts have been based on analysis of long-term gauge (point) measurements of precipitation (e.g., (Serinaldi et al., 2009); (Shiau, 2006)). However, the spatial distribution of rain gauges is not sufficient to provide reliable and homogeneous estimates of the spatial distribution of precipitation, and hence draughts in a global scale (Easterling, 2012). As is well known, the spatial extent is fundamental for understating the drought phenomena (Andreadis et al., 2005). In addition to rain gauges, hydrological and climate model simulations have also been used to assess changes in drought occurrences and intensities ( e.g. (Robock et al., 2004), (Sheffield et al., 2004), (Dirmeyer et al., 2006), (Anderson et al., 2011), (Wehner, 2012)). Climate/hydrological models provide valuable gridded information on droughts and can be used for predicting future scenarios. However, numerous studies have shown discrepan-

cies in regional and global climate models simulations of precipitation patterns and thus drought spatial extent ((WCRP, 2010); (Kirono and Kent, 2011); (Coelho and Goddard, 2009).

Recent advances in developing global satellite precipitation data sets (e.g., (Adler et al., 2003); (Sorooshian et al., 2011b)) provide the opportunity to assess changes in the spatial extent of droughts in the past three decades. The advantages of satellite precipitation data for drought monitoring include: (a) consistent and homogeneous data in a quasi-global scale; (b) coverage over areas with no other means of observations (e.g., rain gauges and weather radars). The importance of using the emerging satellite data sets for drought monitoring, especially for validation and verification of model simulations, has been highlighted in previous studies (e.g., (Wardlow et al., 2012)). The first part of this study analyzes the spatial patterns of droughts using a product combined from multiple satellite precipitation and observations.

The ability to provide gridded precipitation information on a finer scale makes climate models an important tool to assess, monitor and, especially predict drought scenarios. Recently, the Climate Modeling Intercomparison Project Phase 5 (CMIP5) simulations have provided multi-model simulations of the past and future (Taylor et al., 2009). In a recent study, (Alexander and Arblaster, 2009) assessed observed and modeled climate extremes and highlighted the importance of validation and verification of climate simulations with historical observations. Historical monthly precipitation simulations from 41 CMIP5 are processed for analysis for droughts from 1901 to 2005. These data sets represent the most multi-model simulations of historical climate conditions that contribute to the World Climate Research Programme's CMIP multi-model dataset (Meehl and Bony, 2011); (Taylor et al., 2012) . In the second part this study focuses on how well the CMIP5 models replicate results from a validated and verified observed data set on a global and monthly scale.

## 1.2 Aim

The objectives of this thesis, is to use statistical tools in analysis of global drought from various data sets. Primarily, the aim is to investigate changes in spatial extent of areas experiencing drought conditions on a global scale, using satellite data, gauge data and data from CMIP5 models, compared on a monthly basis. For the first part, using satellite-based drought data over the last three decades, we directed our efforts to investigate the following questions: (1a) how areas in meteorological drought have changed and (1b) what regions of the world show wetting and drying trends during this period of time. The second part of the study addresses the following research questions: how well

CMIP5 climate simulations replicate: (2a) area under droughts based on Climate Research Unit's (CRU) observations; and (2b) significant trends in the spatial extent of droughts; and (2c) wetting and drying regions in historical droughts as represented by observations.

### 1.3 Scope and Structure of Thesis

The focal point is to investigate trends and patterns from a statistical point of view. However, the dynamic features responsible for the results are considered to be beyond the scope of this thesis. After this introduction, a theoretical chapter follows, containing a brief overview of the hydrological cycle, teleconnections, drought definitions along with various drought indices and measurements of responding parameters. In Chapter 4, a short introduction to the data sets and models used in this study is given, followed by a chapter on methodology. In chapter 5, the results for the two data sets are analyzed separately to avoid confusion, and the conclusions are likewise presented separately and followed by an overall conclusion together with some comments on future work.

## 2 Theory

Drought development is a slow and complex process that can be described using multiple indicators and variables. Documenting changes in droughts requires long-term records of observations with suitable temporal and spatial coverage. A key variable for drought monitoring is precipitation, which is typically used to describe meteorological droughts (a deficit in precipitation; (Hayes et al., 1999). In the IPCC (2012), it is mentioned that the confidence level of trends in drought development since the 1950s are medium to low, often due to the many areas where evidence is inconsistent or insufficient. The reason for the inconsistency is how results vary depending on model and dryness indices used. Hence it is of large importance to understand the various indices, models and responding parameters used in drought analyses, along with their advantages and disadvantages.

### 2.1 Definition and Description of drought

Development of droughts is a slow and very complex process. Thus, the causes and mechanisms involved are still not fully understood. Among the contributing factors of drought development are precipitation, evapotranspiration and soil conditions. All those are in turn affected by climate, winds, long-time atmospheric and oceanic oscillations. There are multiple types of droughts, and

even though no official definition is agreed upon the following types are generally accepted (Wilhite and Glantz, 1985) in (Fleig et al., 2006).

- Metrological drought = Deficit in precipitation
- Agricultural drought = Deficit in soil moisture, affects vegetation and food production. Also increases the risk of forest fires as vegetation is dryer.
- Hydrological drought = Deficit of surface water and/or ground water. Reduces drinking water supply, hydropower possibilities and water for industrial needs. Affects wild life and humans alike.
- Socio-economical drought = a measurement of impact of droughts, including supply and demand. Usually expressed as economical value. (Wilhite and Glantz, 1985) in (Fleig et al., 2006)

According to (Fleig et al., 2006) the development of droughts may start as a metrological drought initially, and thereafter become an agricultural drought and, if storages are not refilled, develop into a hydrological drought. An analysis of metrological droughts patterns may give information about initial stages of droughts. This thesis focus on meteorological droughts, defined as a lack of precipitation (Fleig et al., 2006), (Hayes et al., 1999).

### 2.1.1 Drought versus aridity

First, the essential difference between the natural hazard *drought* and the climate feature *aridity* should be mentioned. Both describe dry conditions for a region, but while drought is a temporal anomaly from normal conditions, aridity is a constant climate feature. As both drought and aridity can be defined from similar parameters such as precipitation, available water or humidity, awareness on how the parameters are analyzed is vital (Heim, 2002). Statistical indices defined as anomalies from normal conditions are therefore useful when investigating droughts, while absolute methods must be considered in the definition of arid climate regions. Köppen's definition of climate zones are using absolute threshold of precipitation and temperature to define climate zones (Peel et al., 2007). Consequently, while aridity is restricted to certain regions, usually with low precipitation and/or high temperatures, droughts can occur is all climate zones, as it is a condition that deviates from the normal conditions of the region (Heim, 2002).

### 2.1.2 Drought characteristics

Various characteristics can be used to describe droughts. Wilhite (2005) uses three characteristics, intensity, duration and spatial coverage. Intensity describes the magnitude of deficiency while duration is defined as the time of said deficiency, and spatial coverage the area experiencing a deficiency at a certain point of time. Spatial coverage and intensity changes with time as the drought develop. Severity can be described as a product of duration and intensity (Andreadis et al., 2007), and is frequently associated with the vulnerability of an area to drought. Severity can also be defined as the socio-economic impact of droughts, often expressed in economical values of lost production or other costs affiliated with droughts. Finally, severity is also used in indices to distinguish the different phases, for example in the Palmer Drought Severity index 2.4.2.

## 2.2 Hydrological Cycle

### 2.2.1 Processes of the Hydrological Cycle

In regard to drought occurrences and development, the fluctuations and changes in the global hydrological cycle are of great importance and a brief overview of the hydrological cycle is given below. In Figure 1 is the terrestrial water balance shown (Oki and Kanae, 2006). As can be seen (boxed numbers) the largest storage of water is the ocean followed by glaciers and snowpacks along with ground water storage. Other storages for water is, in order of decreasing storage, permafrost, lakes, soil moisture and wetlands, water vapor in the atmosphere and biologically bound water. Accordingly, the largest water fluxes are related to the largest storage, the ocean, and are evaporation from the oceans surface and precipitation over oceans. This is not a closed water cycle as water is transported into the oceans in both subsurface and surface flows. Due to the atmospheric circulations the water evaporating from the oceans move and mix as water vapor, and the overall flux of atmospheric water is towards land areas (Oki and Kanae, 2006). Water is released to the atmosphere through transpiration from vegetation, and from open water surfaces and soil, water is released through evaporation, driven by the heating of the water from sun radiation. Together the processes are referred to as evapotranspiration, one of the most important parameters when investigating droughts. Much research in the field of drought has been focused on how to incorporate evapotranspiration in drought indices (e.g. (Vicente-Serrano et al., 2010); (Dai, 2011); (Sheffield et al., 2012)). Anthropogenic fluxes in the hydrological cycle are for example extraction of water for domestic, industrial and agricultural needs (including irrigation). In comparison to other fluxes those may be small, but they are large enough to have impact

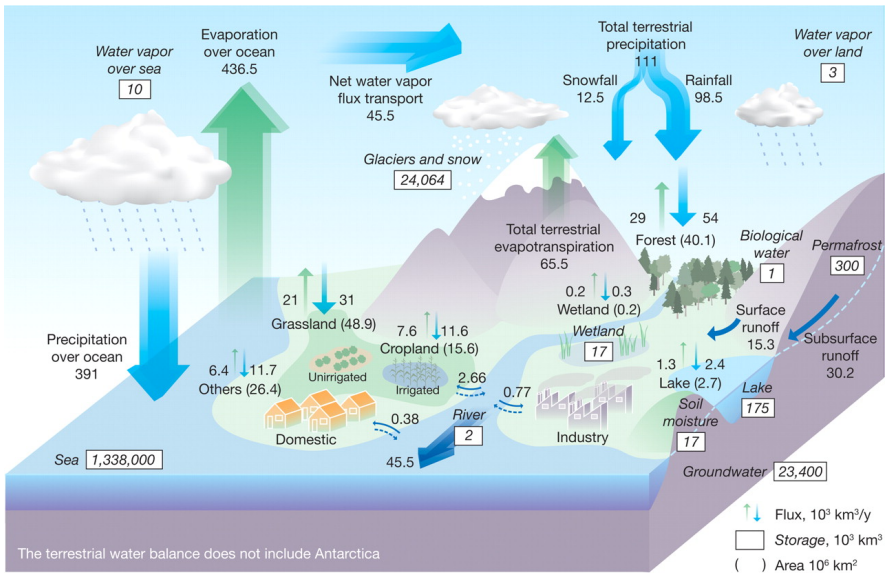


**Figure 1:** The terrestrial water balance illustrates the connections within the hydrological cycle, the driving processes along with absolute values of fluxes to give the relationships between flux and storages(Oki and Kanae, 2006)

on the hydrological cycle and on drought development, excessive water extraction at one point may cause a deficit in sub surface or surface flows and thus agricultural or hydrological droughts may follow (Oki and Kanae, 2006). There are also feed back mechanisms affecting the hydrologic cycle not yet understood, primarily regarding the carbon cycle and cloud mitigation. One of the aims of the fifth phase of CMIP (see 3.4) is to investigate those feed-back mechanisms and their response to various climate scenarios (Taylor et al., 2012).

### 2.2.2 Changes in the Hydrological Cycle

Hydrological processes leading up to droughts, are part of the hydrological cycle, hence drought is responding to changes therein. Many studies address how the hydrological cycle may respond to possible, natural or anthropogenic, changes in climate ((Trenberth et al., 2003); (Oki and Kanae, 2006); (Huntington, 2006)). The general consensus, according to (Huntington, 2006), is that during the 20th century there was an increase in temperature and precipitation over land areas and that those increases will result in an intensification of the hydrological cycle. The theoretical background for the hypothesis is that the Claudius - Clapyeron

relationship implies an exponentially increased in specific humidity in relation to increasing temperature. Overall, the empirical evidence display trends of various parameters indicating an intensification of the water cycle, however, not enough consequent support of increasing extreme weather due to this intensification is reported as there is a lack of consistent and spatial comparable results, according to Huntington (2006). So far no consensus has been reached in this important field of ongoing research (Wood E.F. and Sheffield J., 2012).

## 2.3 Teleconnections

As changes in the hydrological cycle are causing drought development, and the hydrological cycle in turn is affected by atmospheric and oceanic circulations that have been found to affect drought patterns also in areas far from the originating pressure centers. Research has long been conducted in the field of large-scale patterns and their influence on weather over large distances, also known as teleconnections. Teleconnections were first mentioned in 1935 but according to Panagiotopoulos et al. (2002) there still is no distinct definition of the term. The term usually characterizes semi-permanent anomalies in the atmosphere or the oceans that are statistically related to each other. The anomalies are generally described as pressure centers with opposite signs, connected even if situated at geographically large distances. The connections are atmospheric or oceanic and described with changes in wind directions or oceanic currents due to pressure differences. Currents and winds can affect climate over large regions. To study teleconnections many indicators have been used during the years, for example sea level pressures, geopotential heights and surface air or sea surface temperatures (Panagiotopoulos et al., 2002). A challenge in the field has been the arbitrary naming of the patterns, where some patterns go by multiple names and other names are shared between many patterns. Overall, the use of time series analysis has confirmed the majority and indicate that most of them are independent from each other, with the exception of three patterns that share a common center in the the north-east Pacific ocean (Panagiotopoulos et al., 2002).

### 2.3.1 Teleconnections and Drought

Many studies during the years have mentioned a correlation between teleconnections and droughts, and there has been correlations of droughts and some patterns. The El Niño/Southern Oscillation (ENSO) is most analyzed and correlated with drought occurrences. El Niño is defined as increased sea surface temperatures (SST), and the Southern oscillation (also called La Niña) is defined as when anomalies of low SST are detected. According to (Royal Netherlands

Meterological Institute, 2012) the strongest impacts of El Niño with regard to droughts are visible in September to November, when Australia, Indonesia and large part of India along with northeastern Amazonas experience dryer conditions than usual, see FIgure 2. During the Southern Oscillation, the circulation is reversed and areas that experienced wetting conditions during El Niño usually receive less precipitation. Over a year experiencing an El Niño event, the precipitation changes in intensity and other regions experience drought and wetting (Royal Netherlands Meterological Institute, 2012). Correlations between drying over South Asia-Australia, southern Africa and northern South-America, and wetting over central Eurasia, East Africa and South-western US, has been reported in connection to El Niño events (in (Dai, 2011) and (Rajagopalan et al., 2000)). (Dai et al., 2004) concludes that the drying trends, with a 6 month lag, are due to changes in precipitation related to ENSO oscillations. In (Trenberth, 1997) Literature also report correlations between the Asian/Pacific Monsoon

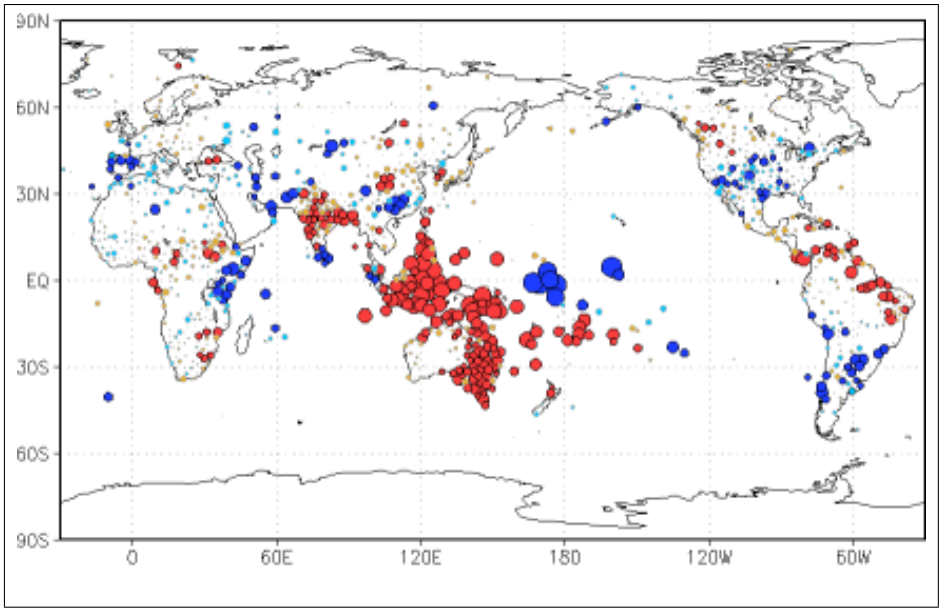


**Figure 2:** Regions of the world experiencing dryer and wetter conditions during an El Niño event, for September to November when the impacts are strongest according to Royal Netherlands Meterological Institute (2012). Red indicate dryer conditions than usual and blue wetter, larger sizes of the circles indicate the strength of relationship. Regions with the largest dry anomalies are eastern Australia and Indonesia although other regions such as the eastern Amazon and India also experience dryer conditions compared to normal (Royal Netherlands Meterological Institute, 2012)

Variability and occurrences of summertime droughts in the United States (Lau, 2000), the Interdecadal Pacific Oscillation (IPO) and droughts in Great Salt Lake, US (Wang et al., 2011), and (Richard et al., 2001) found that changes

in oceanic-atmospheric teleconnection pattern were associated with droughts in Africa.

## 2.4 Drought indices

According to Heim (2002), drought indices were developed simultaneously with the ability of measuring precipitation. The first major drought index is dated to 1916, the Munger's Index, which was created to monitor forest fires and based on number of 24h periods with less than 1.27mm precipitation. Other indices followed, focusing on both short and long term droughts, mainly using precipitation as input, over a specified time scale.

In the 1950s, the evapotranspiration was the first additional aspect of the hydrological cycle to be incorporated when Palmer's Drought Severity Index (PDSI) was developed. Thereafter, indices have attempted to include more parameters, such as subsurface flow, reservoirs storage and water demand. Combinations of indices have also been attempted to describe droughts. For the US a combination of indices is used to create the US drought monitor to monitor and assess droughts at larger scale (Heim, 2002). The performance of drought indices on "hydrological, ecological and agricultural systems"is conducted in Vicente-Serrano et al. (2012), and the authors state that performance of indices varies with local circumstances and with the time scale of interest.

Multiple indices have been developed and are still being developed, and the most common ones, along with the SPI used in the following study, are discussed briefly to give the reader a sense of the multitude procedures available to investigate droughts. Vicente-Serrano et al. (2012) mentions how an abundance of studies using different drought indices reach diverging results, especially when the study correlates with various responding parameters.

The indices mentioned below are selected arbitrarily using some of the review papers published. Many more indices are used locally, regionally and for various purposes. Furthermore, the research on new combined and/or improved drought indices is a continuous process. Table 1 displays a collection of drought indices discussed in details below. Even though this thesis use exclusively the SPI, an account on properties, advantages and disadvantages of other indices are included for understanding of the complexity of drought analysis.

Table 1: Collection of drought index, abbreviations and input parameters used in their computation

| **Abbreviation** | **Full name** | **Input parameters** |
|---|---|---|
| SPI | Standardized Precipitation Index | Precipitation |
| PDSI | Palmer Severity Drought Index | Precipitation and temperature (longer timescale, meteorological drought) |
| Palmers Z-index | Palmer Z-index | Precipitation and temperature (shorter timescale) |
| PHDI | Palmer Hydrological Drought Index | Precipitation and temperature (longer timescale, hydrological drought) |
| SPEI | Standardized Precipitation Evaporation Index | Precipitation and Temperature |
| SWEI | Surface Water Supply Index | Precipitation, Reservoir storage, Snowpack and Streamflow |
| SRI | Standardized Runoff Index | Streamflow |
| VCI | Vegetation Cover Index | Remote Sensing Data |
| vegDRI | Vegetation Drought Response Index | Remote Sensing Data |
| NDVI | Normalized Difference Vegetation Index | Remote Sensing Data |
| NDWI | Normalized Difference Water Index | Remote Sensing Data |
| SMI | Soil Moisture Index | Soil Moisture Content, Wilting Point and Field Capacity |
| DR | Dependable Rain | Precipitation |
| NRI | National Rain Index (Africa) | Precipitation |

### 2.4.1 Standard Precipitation Index

The Standardized Precipitation Index (SPI) is one of the most commonly used and recommended drought indicators ((WMO, 2009): (WCRP, 2010)). SPI ranges from -4 to +4 with negative and positive values indicating drought, and wet periods, respectively. The SPI (McKee et al., 1993) fits a gamma distribution to precipitation data and converts the accumulated probability of the gamma distribution to a normal distribution. Conceptually, the SPI represents how many standard deviations, from the mean value, a precipitation event is for a specific time period. A precipitation frequency distribution has no values below zero, while it displays a higher frequency of precipitation events at lower

intensity. Thus a gamma distribution, with a lower bound at zero and a positive skewness, has a good fit with precipitation data (Thom, 1958). In Figure 3 an example of how precipitation data is fitted to a gamma distribution and a normal distribution is showed. From visible examination of the figure it can be seen that the gamma distribution fits the data better and as this is the usual case, the gamma distribution is used in the development of the SPI(Wilks, 1995).

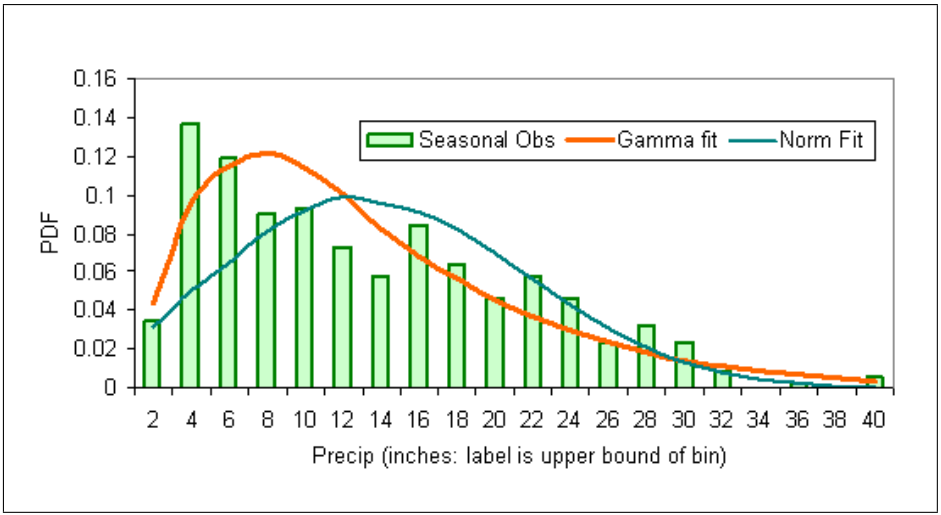


**Figure 3:** Staples of precipitation and the probability density functions (PDF) for normal and gamma distribution. Probability of seasonal precipitation data from Olympia Airport, Washington, US is fitted to a gamma distribution and a normal distribution. A shape parameter of 1.97 and a scale parameter of 6.35 for the gamma distribution was estimated from the seasonal data available (Wilks, 1995)

The gamma distribution is defined by its probability density form in Equation eq 1.

$$g(x) = \frac{1}{\beta^{\alpha}\Gamma(\alpha)} x^{\alpha-1} e^{\frac{-x}{\beta}} \tag{1}$$

where

$$\Gamma(\alpha) = \int_0^{\infty} y^{\alpha-1} e^{-y} dy \quad \text{is the gamma function}$$

$$\alpha > 0 \quad \text{is the shape parameter}$$

$$\beta > 0 \quad \text{is the scale parameter}$$

$x$ is the amount of precipitation

The value of shape and scale parameters can be determined using the maximum likelihood functions (Thom, 1958) for each observation point, each month of the year and each time scale of interest. With the achieved parameters the cumulative probability of a certain rainfall event is computed according to Equation 2.

$$G(x) = \int_c^x g(x)\,dx = \frac{1}{\widehat{\beta}^{\widehat{\alpha}}\Gamma(\widehat{\alpha})} x^{\widehat{\alpha}-1} e^{\frac{-x}{\widehat{\beta}}}\,dx \tag{2}$$

where

$\widehat{\alpha} > 0$ is the optimized shape parameter

$\widehat{\beta} > 0$ is the optimized scale parameter

$x$ is the amount of precipitation

From the accumulated probability function at the selected timescale the results are transformed into a standard normal distribution of random variable Z with a mean of zero and variance of one. The transformation is called an equiprobability transfer a variate from a present distribution to a predefined one and is schematically showed in Figure 4.

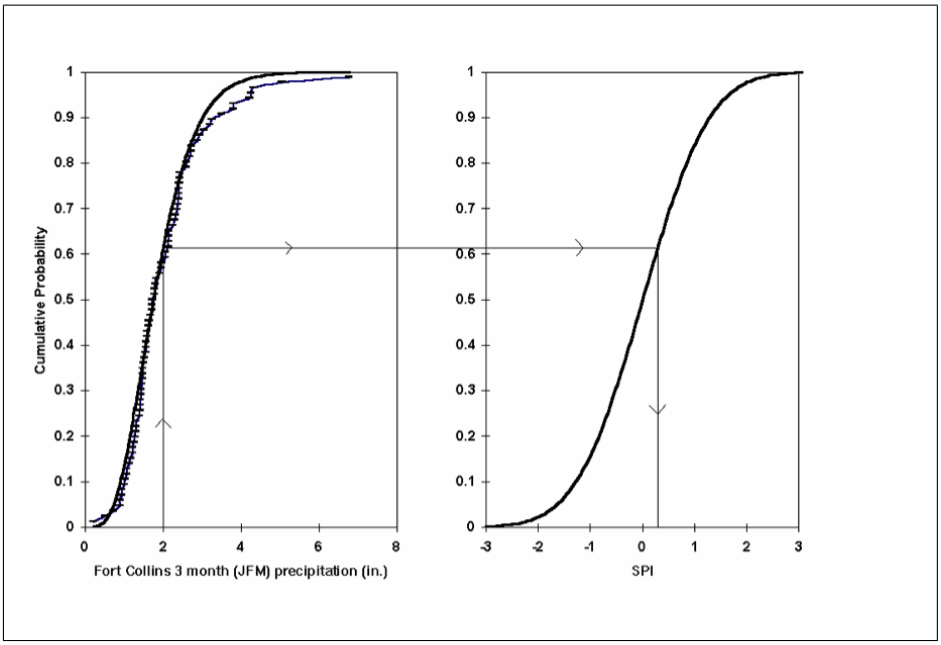


**Figure 4:** To the left is the cumulated probability function plotted for a 3-month precipitation at a station in Fort Collins (dotted black line), fitted to a gamma distribution (smooth black line) and thereafter transformed to a normal distribution in the right panel (Edwards, 1997).

To find the SPI value in Figure 4, find the observation value on the x-axis of the left panel, move in the direction of the arrows vertical up until the curve for the gamma distribution is reached, thereafter move horizontally to the right to the curve in the right panel and from there vertically down to the x-axis) and the SPI-value is read from the x-axis of the righthand panel (Edwards, 1997). To facilitate the use of SPI and not producing those figures for every station at all time scales, a method was developed to approximate cumulative probability, H(x), to a standard normal variable such as SPI. This method was developed in 1965 by Abramowitz and Stegun (Edwards, 1997) and is described in Equations 3 and 4. As can be seen, the Equations 3 and 4 contains approximations ($c_0$, $c_1$, $c_2$, $d_1$, $d_2$ and $d_3$) in order to find the accumulated probability for all cases.

$$SPI = -\left(t - \frac{c_0 t + c_1 t + c_2 t^2}{1 + d_1 t + d_2 t^2 + c_3 t^3}\right) \quad for\ \ 0 \leq H(x) \leq 0.5 \tag{3}$$

$$SPI = +\left(t - \frac{c_0 t + c_1 t + c_2 t^2}{1 + d_1 t + d_2 t^2 + c_3 t^3}\right) \quad for\ \ 0.5 \leq H(x) \leq 1.0 \tag{4}$$

where

$$t = \sqrt{ln\left(\frac{1}{(H\,(x))^2}\right)} \quad for\ \ 0 \leq H(x) \leq 0.5$$

$$t = \sqrt{ln\left(\frac{1}{(1-H(x))^2}\right)} \quad for \ 0.5 \leq H(x) \leq 1.0$$

$$\begin{aligned} c_0 &= 2.515517 \\ c_1 &= 0.802853 \\ c_2 &= 0.010328 \\ d_1 &= 1.432788 \\ d_2 &= 0.189869 \\ d_3 &= 0.001308 \end{aligned}$$

Figure 5 displays the concept of the SPI index. As the index has values of maximum -4 for abnormally dry events and +4 for abnormally wet events, it can be interpreted as how many standard deviations away from the mean a particular event is (Edwards, 1997). According to McKee et al. (1993), SPI values between -1 and -2 incorporate moderate to severe droughts while SPI below -2 indicates extreme droughts.

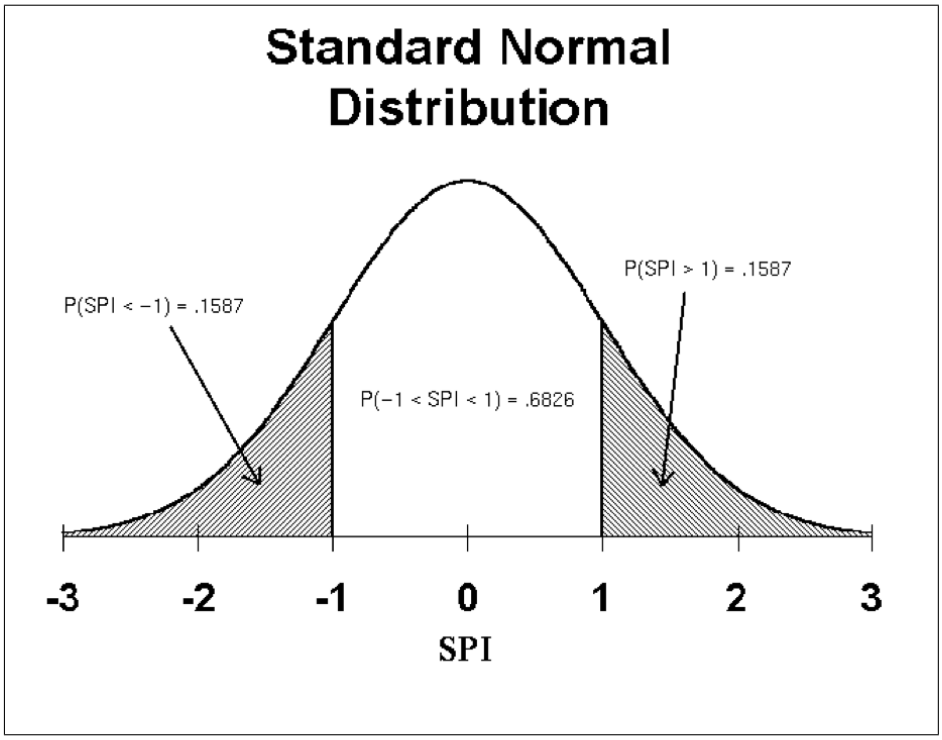


**Figure 5:** Standard normal distribution with the SPI having a mean of = and a variance of 1. The area below -1 represent areas in moderate to severe drought conditions for the future studies citep.

The SPI has the advantage of allowing comparisons over various time scales as well as over different regions. Given the flexibility and simplicity of SPI, it has been widely used in drought studies (e.g., (Mo, 2008), (Wang et al., 2011); (Hao and AghaKouchak, 2012); (Shukla and Wood, 2008)). As mentioned in Vicente-Serrano et al. (2012) two assumptions are included in the SPI is that; a) precipitation varies more than other variables affecting drought (such as evapotranspiration, temperature etc) and b) precipitation is the only variable changing considerably with time. Furthermore, the use of SPI assumes independent observations of precipitation, as all statistical analysis's using distributions are assuming independent observations. There are some limitations connected to the SPI worth mentioning. The use of a gamma distribution in the calculation of the SPI is affected by the length of the precipitation data available, thus requiring longer time series to be applicable (Mishra and Singh, 2010). In some studies other distributions such as the Pearson Type III, lognormal, and exponential distributions SPI values have been used and the results are not comparable between studies. Another limitation mentioned by Mishra and Singh (2010) is how dry climate zones, with extremely low precipitation, can give too many similar values of no precipitation, and thus not fulfilling the normal distribution which is assumed for the index to work. Short data sets especially are vulnerable to this problem. As a concluding remark it should be emphasized that the SPI is a measurement of meteorological drought and thus does not consider effects from evapotranspiration, soil conditions or any other climate variables.

### 2.4.2 Palmer Drought Severity Index

First presented in 1965 , and often said to have revolutionized the drought research, the Palmer Drought Severity Index (PDSI (Palmer, 1965)) is one of the longest used indices for drought monitoring (Vicente-Serrano et al., 2012), (Dai, 2011), (Mishra and Singh, 2010). According to Andreadis et al. (2005) the PDSI is also one of the most widely used drought index, at least for long-term drought characterization.

In similarity with the before mentioned SPI, the PDSI expresses drought, with the value of zero corresponding to normal conditions while negative values indicate droughts and positive values indicate abnormally wet periods (Heim, 2002). The main differences between the two indices are the incorporation of evapotranspiration (as temperature) and soil properties in the PDSI while SPI solely uses precipitation data. In using the additional parameters the PDSI can link meteorological drought with hydrological and agricultural drought (Andreadis et al., 2005).

The PDSI was developed in an attempt to include all processes of the hydrological cycle in a drought index. Due to the complexity of the hydrological cycle there are assumptions included in the PDSI, primarily on moisture transfer. Some assumptions often mentioned and discussed are a) that the top layer of the soil must be fully saturated before infiltration occurs and b) that no runoff is created until both soil layers used in the model are fully saturated (Heim, 2002).

The procedure to calculate the PDSI is that the potential and actual values of four parameters (evapotranspiration (ET), recharge (RC), runoff (RO) and loss(L) ) are retrieved from climate and soil information. To compute the evapotranspiration the Thornthwaithe equation (developed in 1948 and based on temperature information) is used. Thereafter the water balance in Equation 5 is set up to compute the moisture departure ($d$) as a difference between actual precipitation (P) and potential precipitation ($\hat{\text{P}}$) needed to maintain soil moisture(Wells et al., 2004).

$$d = P - \widehat{P} = P - + (\alpha\_iPE + \beta\_iPRC + \gamma\_iPRO - \delta\_iPL) \tag{5}$$

where

$$\alpha, \beta, \gamma, \delta$$

are weighting factors defined as the relationship between the actual parameter and the potential value of the parameter.

As $d$ is specific for each location and time step, Palmer used a correction method to allow comparisons over space and time. A climatology characteristics is created to account for the climate of the region and seasonal changes. With $D$ notating the average moisture department for month $i$ the $K$ is calculated as in Equation 6 (Wells et al., 2004).

$$K_i = \frac{17.67}{\sum_{j=1}^{12} D_j K_j^{'}} K_j^{'} \tag{6}$$

where

$$K_i^{'} = 1.5 \log_{10} \left( \frac{\frac{PE_i + RC_i + RO_i}{P_i + L_i} + 2.8}{D_i} \right) + 0.5$$

The Z-value is the product of the climatology characteristics and the moisture departure and is sensitive to short time anomalies. Long term PDSI is computed according to Equation 7, where the PDSI value of previous months are considered as well as the Z-value, thus giving information on a longer timescale. Thresholds have been set for when a drought or wet spell is considered to

start and end using this equation. The Palmer Hydrological Drought Index, is calculated as the PDSI but with harder restrictions on the thresholds in order to represent hydrological droughts (Karl, 1986).

$$PDSI_i = PDSI_{i-1} + \frac{1}{3}z_i - 0.103PDSI_{i-1} \tag{7}$$

In Dai (2012) various methods to calculate evapotranspiration and handle the calibration of PDSI are discussed and good correlations with observations are obtained. In Sheffield et al. (2012) the authors discuss the use of Penman-Monteith equation, based on radiation influenced parameters, such as wind speed and heat fluxes, to obtain the evapotranspiration. They conclude that the results show overestimations of historical droughts when the original Thornswaithe equation has been used, as only considering temperature makes the evapotranspiration oversensitive to temperature changes (Sheffield et al., 2012).

Mishra and Singh (2010) mentions an additional limitation as the PDSI assume that all precipitation must occur as rain, thus restricting the usefulness to lower altitudes and latitudes, where no precipitation in form of snow occurs. In studies of PDSI and soil moisture (a conventional indicator of agricultural drought) and stream flow (a conventional indicator of hydrological drought), the results indicate that PDSI is indeed unsuited to be used at higher latitudes and during colder periods also due to the impact of snow on evapotranspiration ((Andreadis et al., 2005). Another critique to the PDSI are on the calibration procedures. The calibration includes an empirically computed constant (K') in Equation 6, derived from 9 measurement places in 7 different states in the US. The constant aim to allow for comparisons between locations. New ways to improve this calibration has been presented in research (Wells et al., 2004). In Vicente-Serrano et al. (2012) it is mentioned that the good correspondence between annual streamflow and soil moisture on a global scale found in Dai (2011) might be due to the longer timescale and that performance of PDSI diminishes with a shorter timescale. Many other studies show correlations between various PDSI and responding parameters (see 2.5) such as streamflow and tree rings (Vicente-Serrano et al., 2012).

### 2.4.3 Standardized Precipitation Evapotranspiration Index

The Standardized Precipitation Evapotranspiration Index (SPEI) was first suggested in 2010 by Vicente-Serrano et al. (2010) and is one of the newer indices. It was developed as an attempt to include temperature data in the SPI. It is a probabilistic approach similar to the SPI, but including temperature along with precipitation information. The climatic water balance includes accumulating de-

ficit/surplus of water on multiple timescales and can thusly capture droughts on many time scales. On a global and monthly time scale the authors claim that the SPI and the SPEI perform better than the PDSI (Vicente-Serrano et al., 2012).

### 2.4.4 Surface Runoff Index

Yet another index reminiscent to the SPI is the Standardized Runoff Index derived by Shukla and Wood (2008) and is used to describes hydrological drought. This index is mentioned to be a complement to the SPI on monthly to seasonal timescales as it incorporate seasonal stream flow losses or accumulations (Mishra and Singh, 2010). The index is created in the same way as the SPI, with fitting a gamma distribution to data, and then transforming the cumulated probability function to a normal distribution. As the index incorporates the hydrological response of the area Shukla and Wood (2008) argues that the SRI can be helpful in local drought assessment, especially in areas where the snowmelt seasons are important. On the use of the SRI in forecasts the authors mean that the predictability improves as hydrological initial conditions are included. However, the SRI is hard to evaluate on a larger scale due to restrictions of records (Shukla and Wood, 2008). The challenges and methods of measuring surface runoff are further discussed in Chapter 2.5.4.

### 2.4.5 Surface Water Supply Index

Surface Water Supply Index (SWSI) is an index from 1982 specifically developed to investigate hydrological abnormalities by Shafer and Dezman (Mishra and Singh, 2010). The input variables were reservoir storage, snowpack and streamflow besides precipitation, and from available historical records a non-exceedance probability per month was calculated. Mishra and Singh (2010) states that the Surface Water Supply Index is a good monitoring tool for drought impact on industrial and urban water supplies, irrigation and hydropower generators.

However, as the various factors in the equation are weighted depending on both temporal and spatial scale the index cannot be used in comparison between watersheds or between months. The equation also change snowpack variable to streamflow between seasons, and as seasons changes from year to year it can even be problematic to use the index from year to year (Mishra and Singh, 2010) . Although the index has been found to perform reasonably well with both assessing and predicting water surface supplies in many regions, it was originally empirically developed for Colorado and thereafter modified for other areas, and making it unreliable on larger areas (Heim, 2002).

### 2.4.6 Indices from Remote Sensing Data

The increase of remote sensing data has given the opportunity for researches to develop new types of indices based directly on remote sensing data. Indices looking at the vegetation cover provides information on how vegetation responds to deficit in water, using very high resolution radiometer data (visible and near infrared reflectance from surface to satellite instruments). The technique has been developed from the beginning of the 70's when satellite monitoring started. Positive aspects of the original Vegetation Cover Index (VCI) is the spatial resolution properties and how data can be adjusted for climate, ecology and weather. Drawbacks is that the VCI mainly is useful during summer season as large areas are covered by dormant vegetation during winter seasons. This is especially a problem for the index in temperate climate zones with strong seasons(Mishra and Singh, 2010).

Other indices based on remote sensing data, is the Normalized Difference Water Index (NDWI) and Normalized Difference Vegetation Index (NDVI), also useful for drought assessment. Records of the NDVI is available at a global scale since 1981 at 8km resolution. The NDVI uses the difference between near infrared and visible red reflectance to indicate changes of chlorophyll and intercellular space in plants. High NDVI values reflect a healthy vegetation while lower values show stress on the vegetation for the same timeframe. Both drying and wetting can be shown in with the NDVI. In the development of NDWI the same satellite products are used in combination with shortwave infrared data that makes it possible to retrieve the changes in water content in vegetation (Gu et al., 2008). However, according to Gu et al. (2008) no additional information was achieved in drought assessment by using the NDWI compared to the NDVI. Their results indicated that both indices correlated well with soil moisture (Gu et al., 2008).

In similarity to the NDVI and NDWI, Vegetation Drought Response Index (VegDRI) is a product from the NOAA satellites incorporating information from the Earth Observing Satellites (EOS) of NASA. VegDRI is actually the derivative of the NDVI and is available for the US, producing maps at a very high resolution of $1km^2$ and during the growing season they are updated every week (Brown et al., 2008). For Europe and Horn of Africa the MERIS Global Vegetation Index (MGVI) is used to derive the Fraction of Absorbed Photosynthetic Solar Radiation (fAPAR) which is known to be closely related to water stress in vegetation. This product is also available at a $1km^2$ grid and is published every $10^{th}$ day European Drought Observatory (2012).

### 2.4.7 Other indices

Many more indices have been developed (see Mishra and Singh (2010) for further examples) and active research in the attempt to improve indices to allow further comparisons over various timescales, climate zones and latitudes. Among other the Soil Moisture Deficit Index(SMDI) and the Evapotranspiration Deficit Index (EDI), both developed by Narasimhand and Srinivan in 2005, and based on simulated output from calibrated hydrologic models on a weekly scale. In 2009 the Soil Moisture Index (SMI) was proposed and included wilting point and field capacity (Mishra and Singh, 2010). Many indices have been developed on a regional scale to monitor and analyze droughts in specific areas. For Africa, an index called Dependable Rains, based on the statistical rainfall occurring four out of five years in 1993 and a year later it was turned into the National Rainfall Index (RI). The RI was calculated from rain gauges at a national level and was mainly used for distinguishing patterns at a local scale. Another regional attempt to monitor droughts is the Australian Drought Watch System is based on consecutive months with precipitation below a threshold (Heim, 2002). In the US a Drought Monitor incorporating multiple indices and observation sets (Svoboda et al., 2002).

## 2.5 Measurements of Responding Parameters

As direct drought measurements are impossible, many responding parameters have been used to monitor droughts in a statistical way. Often responding parameters are compared to normal values, or average values over time, to distinguish droughts, either as indices or percentiles. Those responding parameters can both be measured at sites and retrieved from hydrological models. Below some measurements and responding parameters are discussed in short, for the reader to further comprehend the many steps incorporated in analyzing drought. Before a statistical investigation of any kind can be performed the input data needs to be retrieved in a reliable fashion. Many models are producing and/or using the responding parameters for validation which makes the measurement methods essential.

### 2.5.1 Precipitation

Precipitation is the the main input to drought indices (See Table 1) and is also crucial for hydrological models (Behrangi et al., 2011). Having long, uninterrupted precipitation records at global scale are essential for reliable drought monitoring (Easterling, 2012). The oldest method to measure precipitation are rain gauges, available in many forms, from the simple graded cup to automated

weighting stations, but their spatial distribution globally is uneven as is shown in Figure 6. To improve the precipitation record globally use of (a) radar stations, (b) climate models and (c) satellite data. All those methods are currently used to produce precipitation data. Radar requires radar stations and encounters the same disadvantages as gauges, few radar stations available in developing countries and inaccessable areas. Mountain blockage is another reason for gaps in the spatial distribution of the global radar record. Hydrological models can give valuable precipitation information for land areas but require reliable observations to determine boundary conditions. Precipitation records based on satellite data are developing towards finer temporal and spatial resolution but are not available at the scale required for some applications in hydrology yet (Sorooshian et al., 2011a).

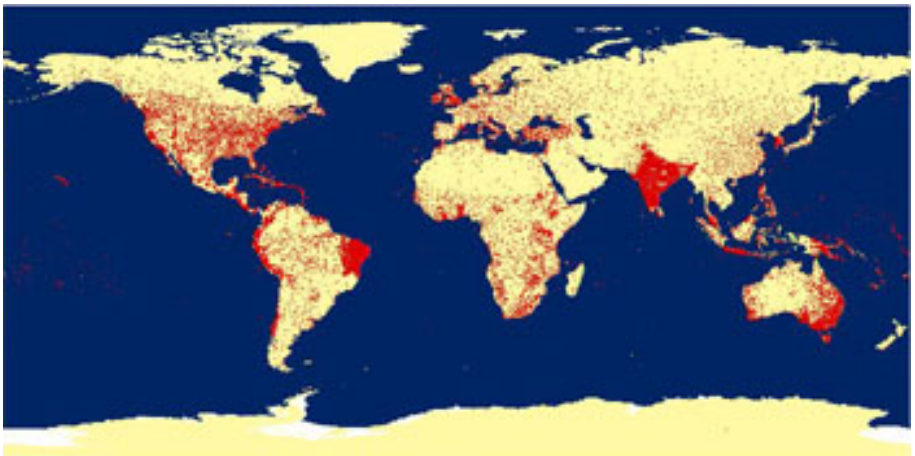

**Figure 6:** Spatial distribution of rain gauges over the globe. Note the uneven distribution between various areas (Center for Hydrometeorology and Remote Sensing, 2004)

### 2.5.2 Groundwater

The level of groundwater wells have been used as an indicator for hydrological droughts. A groundwater investigation is usually performed for a smaller area, such as a basin or an aquifer, and is a massive undertaking as not many data set are available. However, a longterm record of water surface measurements *in situ* are invaluable, especially in detailed model studies to monitor and predict changes in the groundwater (Famiglietti et al., 2011). In a recent study from Famiglietti et al. (2011) data from the Gravity Recovery and Climate Experiment satellite mission (GRACE) satellites enables measurements of the ground water storage using gravimetric data.

### 2.5.3 Soil moisture

Numerous studies define droughts as a percentile of soil moisture compared to seasonal climatology. As soil moisture captures the transpiration from vegetation in addition to precipitation it can be said to represent agricultural droughts (Sheffield and Wood, 2008). For example Sheffield and Wood (2008) use this technique as it is possible and even easy to generate the soil moisture from models. There are a multitude of commercial measurement instruments and soil moisture sensors available today, using various techniques such as neutron scattering, gamma ray attenuation and soil electrical conductivity infra-red absorption and transmission. Main advantage of those methods are that they, in contrast to the thermogravimetric method (drying and weighing of a soil sample in laboratory), are non destructive and can give longer soil moisture records at every site(Walker et al., 2004).

### 2.5.4 Stream flow

Considering streamflow as a lagged integral to the total run off of a basin, long term records of streamflow represent the water availability over time along with the horizontal water flux in the region (Milly et al., 2005). At the Global Runoff Data Centre (GRDC), operating under the World Meteorological Organization (WMO), a database with daily or monthly collected stream flow information from more than 8000 stations in 157 countries with an average record length of 40 years (Global Runoff Data Center, 2008). The spatial distribution of measurement stations and end year for time series is visible in Figure 7. Streamflow discharge usually is computed from continuous elevation measurements using a location specific equation the challenge is to keep the equation updated as banks and stream beds change. The introduction of the acoustic Doppler current profilers (ADCPs) has decreased the time for *in situ* analyses of stream flow and also enabled continuous measurements as the ADCP can be fixed. Placing technical equipment in water is affiliated to risks of disturbances in the records, as unplanned events like debris, high flow etc may occur, and in response to those risks research on using remote sensing data to record streamflow is under investigation (Hirsch and Costa, 2004).

### 2.5.5 Tree rings

The use of tree rings can give information on droughts as the width of tree rings changes depending on availability of water. This gives a distinct difference between growth and dormant seasons over the year, and when water is scarce the growth of the tree is affected and can be distinguished. Tree ring reconstructions can be used as a drought information for times without any other

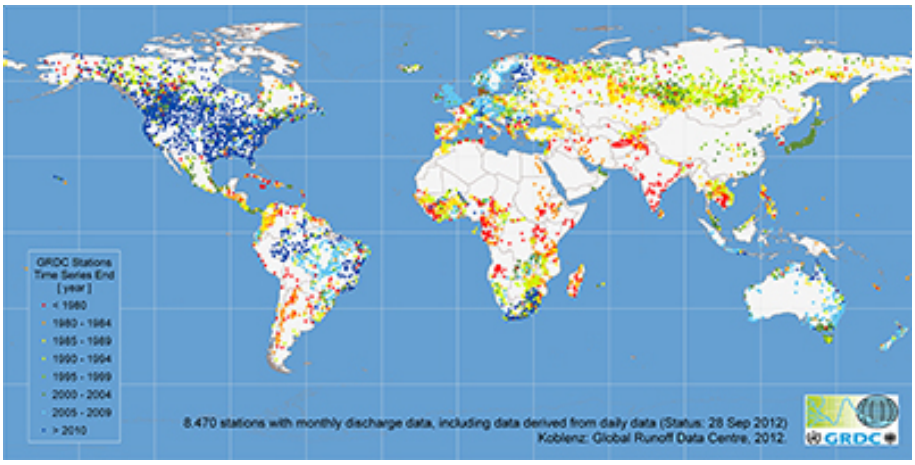


**Figure 7:** Spatial distribution of stations reporting run off to GRDC and indications on end year for reported observations (Global Runoff Data Center, 2008)

precipitation record available(Mishra and Singh, 2010). However, the widths of tree rings are only a good indicator of droughts in areas where water abundance is the governing factor, such as arid areas. Studies of humid areas indicate lower correlation between tree rings width and droughts (Vicente-Serrano et al., 2012).

### 2.5.6 Crop yield

Vicente-Serrano et al. (2012) investigated the correlation of drought indices with the crop yields globally. The largest correlation were recorded in semi-arid areas where large surfaces were cultivated with mainly wheat, such as Russia, Australia and Spain. In another areas of the globe humid climate or well developed irrigation system might have reduced the vulnerability of water scarcity (Vicente-Serrano et al., 2012). In Mishra and Singh (2010) crop yields are mentioned to correlate well with large scale climate phenomena such as ENSO in the US and Australia. Crop yields assessment can be carried out from various satellite measurements such as NDVI, NDWI and VegDRI ( see 2.4.6).

# 3 Observations and Models

As this analysis is using the SPI (see Chapter 2.4.1) precipitation data information is used as input. Two kinds of precipitation data has been used, both precipitation data based on remote sensing and adjusted with gauge data and precipitation data generated by climate models. Below the remote sensing data

used is presented and followed by some information about the climate models used.

## 3.1 Remote Sensing Data

Having long-term precipitation data is fundamental to reliable drought analysis. As satellite records emerge and their results improve a new possibility of model independent data, that can be used to validate and verify models, evolve (AghaKouchak et al., 2012). From the beginning of the millennium, several satellite-based products available in real-time on a finer resolution provide global precipitation estimates (e.g., Tropical Rainfall Measuring Mission (TRMM) Multisatellite Precipitation Analysis (TMPA) (Huffman et al., 2007); CPC Morphing Technique (CMORPH) (Joyce et al., 2004); and Precipitation Estimation from Remotely Sensed Information using Articial Neural Networks (PERSIANN) (see Chapter 3.1.2). One of the limitations of real-time satellite-derived precipitation estimates is their relatively short length of data (currently 10-13 years). One long-term precipitation estimate reaching back to 1979, but with a lag in real time, is the gauge adjusted Global Precipitation Climatology Project (explained in detail in Chapter 3.1.1). Even though a large effort is made to statistically validate satellite products there are still improvements needed in various fields, for example on pattern recognition (AghaKouchak et al., 2011)and on bias correction algorithms Behrangi et al. (2011). According to AghaKouchak et al. (2011) the lack of information regarding reliability and uncertainties of most real-time products, they are not integrated into application outside the research community yet. Here follows a presentation of the precipitation data sets used in the study along with an overview of the multimode set used.

### 3.1.1 Global Precipitation Climatology Project

As an international effort to further investigate the understanding on the energy and water cycles the Global Precipitation Climatology Project (GPCP, (Adler et al., 2003)) was initiated as one of many components of the Global Energy and Water Experiment (GEWEX) by the World Meteorological Organization (WMO) and the World Climate Research Programme. The GPCP is currently maintained and developed for the international research community on behalf of the WMO, WCRP and GEWEX. Input data are provided by scientists and research groups from all around the world, and GPCP incorporates information from many countries as can be seen in Table 2. The final product is produced by a group led by R. Adler and G. Huffman from NASA's Goddard Space and Flight Center (GSFC) and the dataset is constantly improving as remote sensing technique and gauge data analyses improve. The GPCP product is currently

available at a $2.5^o$ grid for monthly data, starting in 1979, and data is available at a 5-days period and, from 1996, as a daily product at a $1^o$ resolution (Huffman et al., 2009).

Table 2: Input data used for producing GPCP (Huffman et al., 2009)

| **Input Data** | **Organization providing Data** | **Processed and contributed by** |
|---|---|---|
| Special Sensor Microwave/ Imager Data (SSM/I) | Defense Meteorological Satellite Program, U.S.) | L. Chiu (Chinese Univ. of Hong Kong and George Mason Univ., U.S.) and R. Ferraro (National Environmental Satellite Data and Information Service, NESDIS, U.S.) |
| Merged geosynchronous- and low-Earth-orbit infrared (geo- and leo-IR) | NESDIS, the Japanese Meteorological Agency, and the European Organisation for the Exploitation of Meteorological Satellites | P. Xie (National Oceanic and Atmospheric Administration/Climate Prediction Center, NOAA/CPC, U.S.) |
| Outgoing Longwave Radiation (OLR) Precipitation Index (OPI) | NOAA leo-IR data and NESDIS, the Japanese Meteorological Agency, and the European Organisation for the Exploitation of Meteorological Satellites | P. Xie (National Oceanic and Atmospheric Administration/Climate Prediction Center, NOAA/CPC, U.S.) |
| Estimates based on the Television Infrared Observation Satellite Operational Vertical Sounder (TOVS) | NESDIS, the Japanese Meteorological Agency, and the European Organisation for the Exploitation of Meteorological Satellites and the Advanced Infrared Sounder (AIRS; provided by NASA) | J. Susskind (National Aeronautics and Space Administration/Goddard Space Flight Center, NASA/GSFC, U.S. |
| Global precipitation-gauge analyses | Weather stations around the world | B. Rudolf and U. Schneider (Global Precipitation Climatology Centre, GPCC, hosted at the Deutscher Wetterdienst) |

### 3.1.2 PERSIANN

The Precipitation Estimation from Remotely Sensed information using Artificial Neural Networks (PERSIANN, (Sorooshian et al., 2000); (Hsu et al., 1997)) is developed at the Center for Hydrometerology & Remote Sensing (CHRS) at University of California, Irvine and utilizes the technology of neural networks to

map the complicated unlinear functions involved in transferring remote sensing data into a form that can be used in applications. How the process works is showed in the schematics in figure 8, where the first layer is the input layer, then there is a hidden layer and finally an output layer. The layers are connected with weighted links between the nodes of the different layers. Values of the hidden layer depends on the input values and those weighted links and the out put values are linked to the hidden layer accordingly. While training the Neural Network an optimization dataset is used, where both input and output values are known, and optimization algorithms that minimize the difference between observed and desired output give information on the weighted links. In (Sorooshian et al., 2000) a detailed explanation of how the algorithms are used to produce the estimation product, a raster map with a $0.5^o$ x $0.5^o$ grid that is made available as daily, 3 and 6 hrs precipitation on a global scale. The PERSIANN system was based on geostationary infrared imagery (from and later extended to include the use of both infrared and daytime visible imagery (Center for Hydrometeorology and Remote Sensing, 2004).

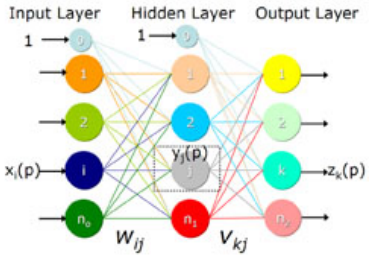


**Figure 8:** Schematics of processes in the learning algorithm of ANN, where the lines between nodes are the weighted links whose weights are decided by optimization algorithms (Center for Hydrometeorology and Remote Sensing, 2004)

## 3.2 Satellite-based Merged Dataset

As the NASA's long-term GPCP precipitation estimate is not available in real-time (presently, the latest data has 20 months latency) it limits application of long-term satellite data in real-time drought monitoring. In a recent study, a merged monthly data set that combines the long-term GPCP satellite data with real-time satellite estimates (TMPA-RT and PERSIANN) has been developed for drought analysis (AghaKouchak and Nakhjiri, 2012). In the merged dataset, the climatology is driven by GPCP data and the near past data (approximately 12-24 months) is based on real-time satellite precipitation data with an overlapping 9 years for calibration and a year for validation (see Figure 9).

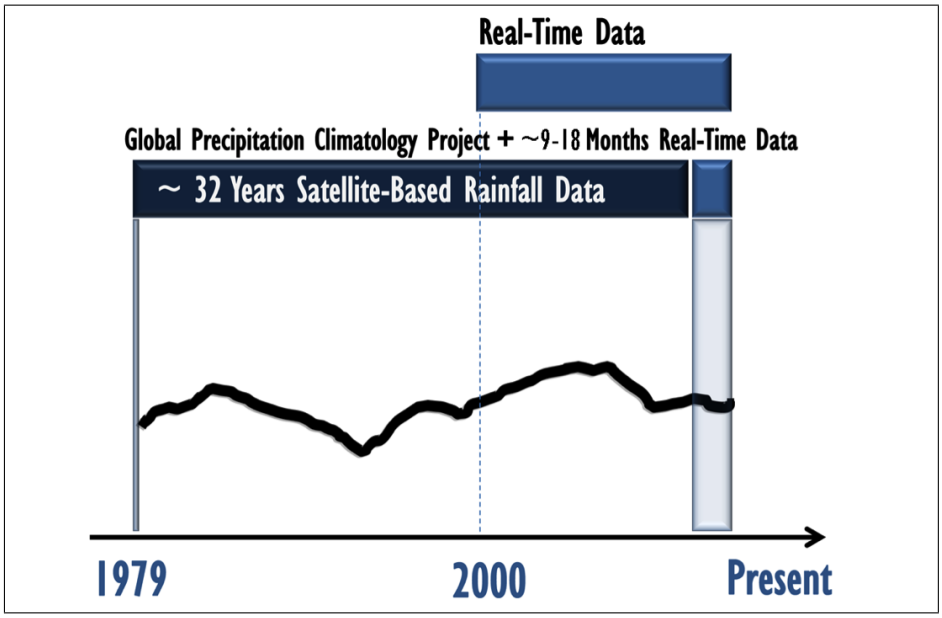


**Figure 9:** Schematics of merging longterm GPCP and real-time satellite products (AghaKouchak and Nakhjiri, 2012)

The merging algorithm includes spatial and temporal bias correction algorithms to ensure consistency of the two data sets for drought analysis. The algorithms and the overall quality of the two data sets are tested and validated for the period of overlap (2000-2010) between GPCP and both TMPA-RT and PERSIANN (see (AghaKouchak and Nakhjiri, 2012)). The final product is a data set of consistent monthly precipitation data with a spatial resolution of $2.5^o$ from 1979 to present. Figure 10 displays example global SPI-based drought maps for several time steps. As shown, some of the recent major droughts such as the Horn of Africa and the Amazon droughts are captured in this data. To capture longer droughts the 6 (intermediate duration) and 12 months (long duration) SPI are chosen, as the base period then is longer.

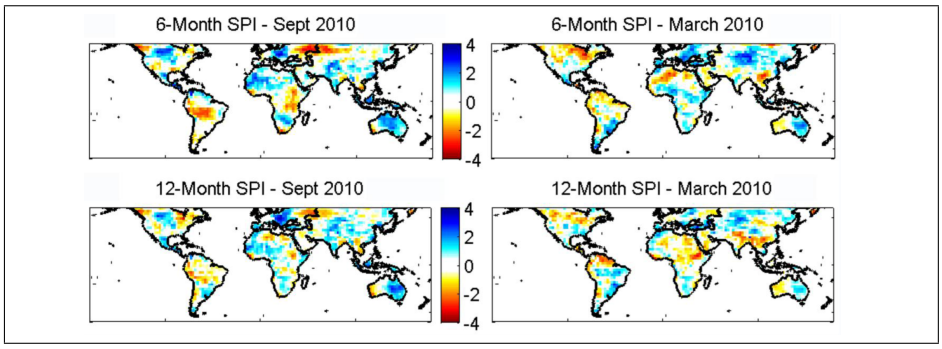


**Figure 10:** Example global maps of SPI over 6 and 12 months. (AghaKouchak and Nakhjiri, 2012)

## 3.3 Observed data from Climate Research Unit

The Climate Research Unit (CRU) at the University of East Anglia, UK provides data sets with climate data that are used both by IPCC and the research community at large. Grids of information for the nine climate variables temperature, diurnal temperature range, daily minimum and maximum temperatures, precipitation, wet-day frequency, frost-day frequency, vapour pressure, and cloud cover are created for the global land areas excluding Antarctica. Observations from weather stations are the base of the informations and interpolation and cross-validations between the stations are performed (Mitchell and Jones, 2005).

## 3.4 CMIP5 models

Precipitation data for the study is also generated from recent simulations of climate models. In 2008, the WCRP's Working Group on Coupled Modeling (WGCM) agreed to promote a new set of coordinated climate model experiments that was to be the fifth phase of the Coupled Model Inter-comparison Project (CMIP5). The goal of the fifth phase is (1) further understanding on feedback related to the carbon cycle and with clouds; (2) investigate predictability on decadal time scales; and (3) find why models using similar forcing produce different responses. In total there are more than 50 models developed by over 20 international groups, however, not all groups are interested in performing the same experiments and therefore certain core scenarios are chosen. There are two required main experimental sets to conduct, either on a long-term (century) scale or near-term (10-30 years, also called decadal prediction) scale, to receive a multimodel set that can be used for comparison between models. One difference between the timescales is the inital conditions, where the decadal experiments starts with observed ocean and sea ice conditions, the long-term experiments usually start with preindustiral conditions (quasi equilibrium). The various experiments are similar to each other, and to previous phases, in the sense that atmosphereocean global climate models (AOGCMs) can be used, but in the fifth phase Earth system models of intermediate complexity (EMICs) can be included. All models, both AOGCMs and EMICs, respond to similar forcings and have representation of ocean, athmospere, land and sea ice. A new feature is that some of the AOGCMs are coupled to carbon fluxes and can compute concentrations of emitted constituents, those models are called Earth system models (ESMs). The AOGCMs and ESMs can be used for both long-term and near-term experiments while the EMICs are limited to the long-term experiments (Taylor et al., 2012)

### 3.4.1 Models used in the Analysis

The models used in this study are available in from CMIP5 database. The simulations are available from 1901 until 2005, as is the observed record. Table 3 show the models participating in this study and their origin. Some visuals only contain a selection of the models, due to the otherwise over whelming amount of figures. The selection is loosely based on (a) at least one model from each modeling group and (b) a calculation of least absolute mean square error compared to the observational dataset. Ensemble mean values of precipitation of all 41 models were calculated and those are called Ensemble mean below and were subjected to similar analysis as the separate models. The models of this study along with the modeling center responsible for their generation are summarized in Table 3.

Table 3: Name and origin of models from CMIP5 used in the analysis

| **Name** | **Origin of model** |
|---|---|
| CRU, observations | Climate Research Unit, East Anglia University, UK |
| BCC-CSM1-1 | Beijing Climate Center, China Meteorological Administration |
| BCC-CSM1-1-esm | Beijing Climate Center, China Meteorological Administration |
| CanESM2 | Canadian Centre for Climate Modelling and Analysis |
| CanESM2-esm | Canadian Centre for Climate Modelling and Analysis |
| CCSM4 | Climate and Global Dynamics Division at the National Center for Atmospheric Research, US |
| CESM1-BGC | Climate and Global Dynamics Division at the National Center for Atmospheric Research, US |
| CESM1-BGC-esm | Climate and Global Dynamics Division at the National Center for Atmospheric Research, US |
| CESM1-CAM5 | Climate and Global Dynamics Division at the National Center for Atmospheric Research, US |
| CESM1-FASTCHEM | Climate and Global Dynamics Division at the National Center for Atmospheric Research, US |
| CESM1-WACCM | Climate and Global Dynamics Division at the National Center for Atmospheric Research, US |
| CNRM-CM5 | Centre National de Recherches Meteorologiques, France |
| CSIRO-ACCESS1-0 | Commonwealth Scientific and Industrial Research Organisation, Australia |

Continued on next page

| Name | Origin of model |
|---|---|
| CSIRO-ACCESS1-3 | Commonwealth Scientific and Industrial Research Organisation, Australia |
| CSIRO-Mk3-6-0 | Commonwealth Scientific and Industrial Research Organisation, Australia |
| FGOALS-g2 | Chinese Academy of Sciences, Institute of Atmospheric Physics |
| FGOALS-s2 | Chinese Academy of Sciences, Institute of Atmospheric Physics |
| GFDL-CM3-esm | Geodynamical Fluid Dynamic Laboratory, National Oceanic and Atmospheric Administration, US |
| GFDL-ESM2G | Geodynamical Fluid Dynamic Laboratory, National Oceanic and Atmospheric Administration, US |
| GFDL-ESM2M | Geodynamical Flud Dynamic Laboratory, National Oceanic and Atmospheric Administration, US |
| GFDL-ESM2M-esm | Geodynamical Fluiid Dynamic Laboratory, National Oceanic and Atmospheric Administration, US |
| GISS-E2-H | Goddard Institute for Space Studies, NASA, US |
| GISS-E2-R | Goddard Institute for Space Studies, NASA, US |
| HadGEM2 | Met Office Hadley Centre, UK |
| HadGEM2-CC | Met Office Hadley Centre, UK |
| HadGEM2-ES-esm | Met Office Hadley Centre, UK |
| INMCM4-esm | Institute of Numerical Mathematics Russian Academy of Sciences |
| IPSL-CM5A-LR | Institut Pierre-Simon Laplace, France |
| IPSL-CM5A-LResm | Institut Pierre-Simon Laplace, France |
| IPSL-CM5A-MR | Institut Pierre-Simon Laplace, France |
| IPSL-CM5B-LR | Institut Pierre-Simon Laplace, France |
| MIROC5 | Atmosphere and Ocean Research Institute and National Institute for Environmental Studies, Japan |
| MIROC-ESM | Atmosphere and Ocean Research Institute and National Institute for Environmental Studies |
| MIROC-ESM-CHEM | Atmosphere and Ocean Research Institute and National Institute for Environmental Studies |
| MIROC-ESM-esm | Atmosphere and Ocean Research Institute and National Institute for Environmental Studies |
| MPI-ESM-LR | Max Planck Institute for Meteorology, Germany |
| MPI-ESM-LR-esm | Max Planck Institute for Meteorology, Germany |
| MPI-ESM-P | Max Planck Institute for Meteorology, Germany |
| MRI-CGCM3 | Meteorological Research Institute, Japan |
| MRI-ESM1 | Meteorological Research Institute, Japan |
| NorESM1-M | EarthClim, Norway |
| NorESM1-ME | EarthClim, Norway |

# 4 Methodology

## 4.1 SPI

In this document, and following Yoon et al. (2012), 6-month SPI is employed to investigate meteorological droughts. The advantages of SPI as a drought indicator have been discussed in multiple studies (Hayes et al., 2011) and it is one of the most commonly used and recommended drought indicators (WMO (2009); WCRP (2010)). The drought conditions used in this study are: (a) -2 $<$ SPI $\leq$ -1 (moderate to severe droughts); and (b) SPI$\leq$-2 (extreme droughts which corresponds to exceptional drought severity in the U.S. Drought Monitor citep(Svoboda et al., 2002)). When interested in droughts overall, as all droughts below SPI $\leq$ -1 are used.

In the first part of the study uses the merged satellite data with a resolution of $2.5^o$ and for the second part the observations and model simulations are re-mapped on to a common 2-degree spatial resolution. The study area is the same for both parts of the study; extending from $60^o$S to $60^o$N where satellite-based data is available. However, there is a difference in temporal scale, the merged satellite data set consist of 32 years of data while the CMIP5 simulations cover 102 years. Following (Sheffield and Wood, 2008), areas with rainfall below 0.5 mm day-1 ($<$15mm/month) are masked out of the analysis to avoid unreliable statistics. This procedure eliminates areas in perpetual droughts such as deserts where a small variability in monthly rainfall changes wet and dry conditions considerably.

The SPI, derived from either the satellite-based precipitation or climate model simulated precipitation and CRU observations, is used to derive fractional area under drought. Each pixels SPI value is computed accordingly to Chapter 2.4.1 and represents the amount of precipitation for any given period with respect to the climatology for the same duration. The generation of SPI used a code developed by Lee (2009) and further developed by Nakhjiri (2012). The original code is available at Matlab's file exchange homepage.

The areas under drought are plotted against time for (a) total land area, (b) land area in the Northern Hemisphere (NH), and (c) land area in the Southern Hemisphere (SH). For the first part of the study the separation of ocean and land was also performed, and all analyses were conducted for the total globe as well as land and ocean separately.

## 4.2 Mann- Kendall's test

In order to investigate trends for the last century in the areas under drought, the non-parametric test developed by Mann (1945) and Kendall (1976) is employed.

The test uses the ranking of all the values to determine if there are more increasing or decreasing values in historical records. In the Mann-Kendall each test value $x_1$ ... $x_n$, are compared with all available values. For a positive difference between the data points the so-called S-statistics increases with +1 while it decreases with -1 for a negative difference. The S-statistics remains unchanged for ties (see equation 8 and 9 ).

$$S = \sum_{i=1}^{n-1} \sum_{j=i+1}^{n} sgn\left(x_j - x_i\right) \tag{8}$$

where

$$Sgn\left(x_j - x_i\right) \begin{cases} +1, > \left(x_j - x_i\right) \\ 0, = \left(x_j - x_i\right) \\ -1, < \left(x_j - x_i\right) \end{cases} \tag{9}$$

and

$$Var\left(S\right) = \frac{n\left(n-1\right)\left(\right)\sum_{i=1}^{m} t_1\left(i\right)\left(i-1\right)\left(i+5\right)}{18}$$

Thus a large positive value of S indicates a strong positive (increasing) trend while a large negative value of S implies a negative (decreasing) trend. The non-parametric assumption of Mann-Kendall′s test when used for a time series with a large number of values is documented to allow the use of a regular z-test to determine whether a trend is significant or not, see 10 (Yue et al., 259):

$$Z = \begin{cases} \frac{S-1}{\sqrt{\frac{n(n-1)(2n+5)-\sum_{j=1}^{q}(t_j)t_j\left(t_j-1\right)(2t+5)}{18}}}, & \text{if } S > 0 \\ 0 \quad \text{if } S > 0 \\ \frac{S+1}{\sqrt{\frac{n(n-1)(2n+5)-\sum_{j=1}^{q}(t_j)t_j\left(t_j-1\right)(2t+5)}{18}}}, & \text{if } S < 0 \end{cases} \tag{10}$$

where $n$ = sample size; $q$= number of tied groups in the data set; and $t_j$ = number of data points in the $j^{th}$ tied group. Throughout this study, the common p-value of 0.05 (95% confidence) or 0.01 (99% confidence) are used as threshold to indicate the

The advantage of the the Mann-Kendall test is that only the rank of the values is used. The test provides information on whether the null-hypothesis of no trend in the data can be rejected based on the rank (Helsel and Hirsh, 2010). The Mann-Kendall test function from Fatichi (2009) returns an H-value of 1 if a trend is detected and the null-hypothesis of no trend is rejected. Consequently, the test returns the H-value of 0 if the null-hypothesis of no trend cannot be rejected at a given significance level (e.g., 0.05 or 0.01). In this study, the Mann-Kendall test was performed both on the time serie of area under drought

conditions as well as on each individual pixel to investigate spatial distribution of wetting and drying trends over time.

To investigate trends in the above time series the Mann-Kendall test ((Mann, 1945); (Kendall, 1976)) is used. The test returns the so-called H-value which is either 0, indicating the null-hypothesis is correct and no trend is detected, or 1, indicating the detection of a trend. In this study, the Mann-Kendall test is performed using the algorithm developed by (Fatichi, 2009). Throughout the study, a significance-level of 0.05 is used for analysis indicating 95% confidence. Finally, the Mann-Kendall test is used to examine trends in each pixel and how areas experience drying or wetting trends from January 1980 to January 2012.

## 4.3 POD

In order to quantify the accuracy of models a probability of detection (POD) value was calculated for each model in comparison to the observation data. Here, the POD is defined as the ratio of land pixels where the trends (whether positive/negative/no trend) are identified correctly divided by the total number of land pixels. NaN values are used for areas in perpetual drought and pixels with no data.

# 5 Results

The results are presented separately for the study based on what precipitation record used. Firstly, the results from the analysis of the 32-year long dataset, based on merged satellite precipitation records, are presented. Therafter, all results from the analysis using data generated by CMIP5 models and CRU observations are presented and discussed.

## 5.1 Results from analysis of the Satellite-based Merged Dataset

### 5.1.1 Area under drought

In the following, the global satellite-based drought data from 1980 to 2012, are used for analysis of global trends and patterns of droughts. Figure 11 and Figure 12 display areas in moderate to severe drought (Figure 11) and extreme drought (Figure 12 ) in the past three decades. Both figures consist of three panels, a) area (%) of the globe, land, land in the NH, and land in the SH under drought condition; b) area (%) of the globe, ocean, ocean in the NH, and ocean in the SH under drought and c) area (%) of the globe, land and ocean under drought. All three panels include the global area in drought (solid black line) for reference.

The results indicate that on average 15 to 16% of the globe is under drought (SPI $\leq$ -1), whereof 2 to 3% is in extreme drought condition. This is consistent with Sheffield and Wood, 2008, which indicated that 20% of the land has been under drought (defined as soil moisture percentage below the 20th percentile) during the past five decades. While the average area under drought for land (15.99%), land in the NH (16.03%), and land in the SH (15.89%) are very similar, droughts over land in the SH are far more variable than those over land in the NH (see Figures 11a and 11b). As shown in Figure 11a, the variability (range of changes) in fraction of land in moderate to severe drought conditions (-2 $<$ SPI $\leq$ -1) is approximately 19% in NH, while it is over 30% in SH. From Figures 11a and 12a one can conclude that in terms of both amplitude and frequency land droughts are more variable in SH than in NH.

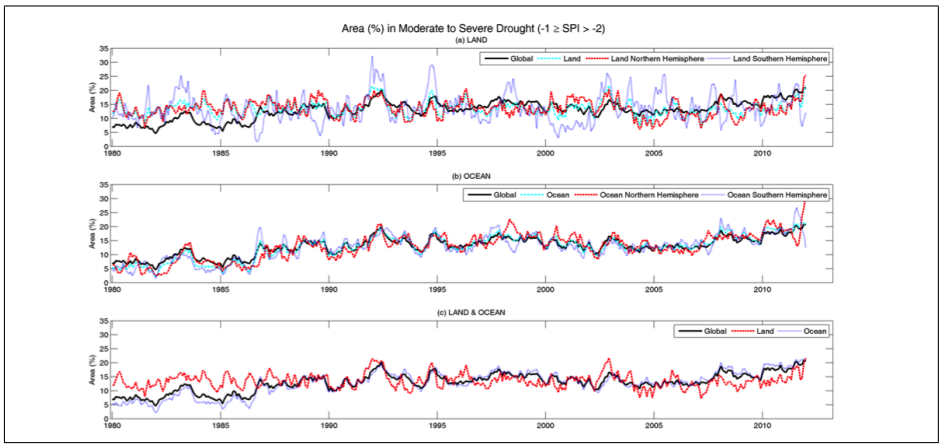


**Figure 11:** Area (%) in moderate to severe drought (-1 $\geq$ 6-month SPI $>$ -2)for a)the globe, all land, land in NH and SH respectively b) the globe, all ocean, ocean in NH and SH respectively c) the globe, all land and all ocean from 1980 to 2012..

As demonstrated in Figures 11 and 12, more peaks of land under drought can be observed in SH compared to NH. However, drought over ocean in NH and SH are more consistent with respect to their area under drought (approximately 15% to 16%) and variability (compare Figure 11a with Figure 11b and Figure 12a with Figure 12b).

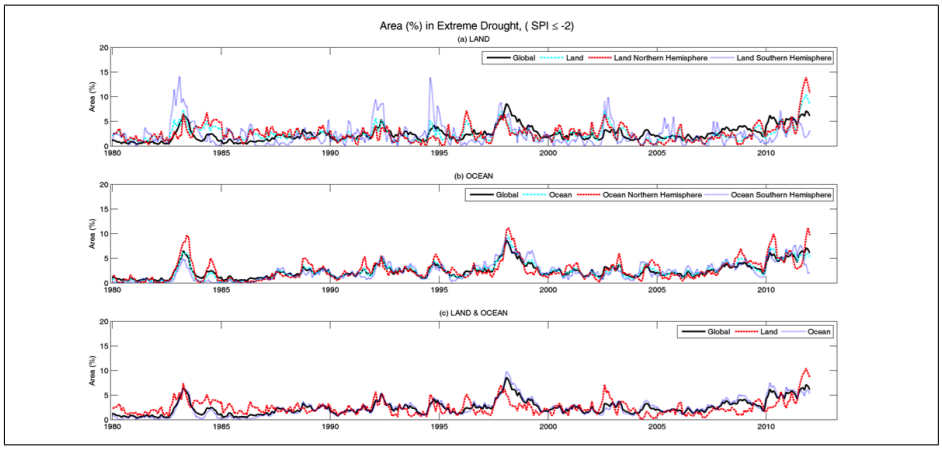


**Figure 12:** Area (%) in extreme drought (6-month SPI $\leq$ -2) for a)the globe, all land, land in NH and SH respectively b) the globe, all ocean, ocean in NH and SH respectively c) the globe, all land and all ocean from 1980 to 2012.

Table 4 summarizes area under drought for different drought severity thresholds. One can see that on average the area (%) of land under drought is slightly (around 1% or less) higher than area of ocean under drought. Table 4 indicates that the area under extreme drought is similar for land, ocean, NH, and SH (approximately 2.5%).

Table 4: Average fraction of area in drought (%), for moderate to severe drought (-1 $\geq$ SPI > -2), extreme droughts (SPI $\leq$ -2) and drought as a total (SPI $\leq$ -1).

| | **-1 $\geq$ SPI > -2** | **SPI $\leq$ -2** | **SPI $\leq$ -1** |
|---|---|---|---|
| Global | 12.94 | 2.47 | 15.40 |
| Land | 13.52 | 2.47 | 15.99 |
| Ocean | 12.74 | 2.47 | 15.21 |
| NH | 13.09 | 2.58 | 15.67 |
| SH | 12.79 | 2.35 | 15.14 |
| Land NH | 13.52 | 2.51 | 16.03 |
| Land SH | 13.53 | 2.36 | 15.89 |
| Ocean NH | 12.80 | 2.62 | 15.47 |
| Ocean SH | 12.67 | 2.35 | 15.02 |

### 5.1.2 Trends in Area under Drought

Table 5 summarizes the Mann-Kendall trend analysis results for drought area (%) over the past three decades, in the analysis based on a merged precipitation record from satellites. In this table, Column 1 shows the H-value where 1 indicates a trend at the significance level of 0.05 and 0 indicates no trend. The P-values in column 2 represent the probability of receiving the values of the data under the null-hypothesis that there is no trend and thus a small P-value

indicates higher confidence. One can see that the area under drought has been increasing over the entire globe and oceans, but not over land. As shown in Table 5, significant trends (H-value = 1) have been observed over the entire globe and oceans. For the analysis, p-values below 0.05 are considered as significant trends (confidence of 95%). A smaller P-value implies more confidence in the presence of a trend. The p-value of trend analysis over land indicates no trend (significant increase) in the area of land under drought in the past three decades.

Table 5: Trends in the area under drought over the past three decades based on the Mann-Kendall test. Column 1 shows the H-value, 1 indicates a trend at the significance level of 0.05 and 0 indicates no trend. The P-values in column 2 represent the probability of receiving the values of the data under the null-hypothesis that there is no trend and thus a small P-value indicates higher confidence.

| | | **H-Value** | **P-value** |
|---|---|---|---|
| Globe | SPI$\leq$-1 | 1 | 0 |
| Land | SPI$\leq$-1 | 0 | 0.799 |
| Ocean | SPI$\leq$-1 | 1 | 0 |
| NH (Land & Ocean) | SPI$\leq$-1 | 1 | 0 |
| SH (Land & Ocean) | SPI$\leq$-1 | 1 | 0 |
| NH (Land) | SPI$\leq$-1 | 0 | 0.156 |
| SH (Land) | SPI$\leq$-1 | 1 | 0.04 |
| NH (Ocean) | SPI$\leq$-1 | 1 | 0 |
| SH (Ocean) | SPI$\leq$-1 | 1 | 0 |

Based on model simulations, Dai (2011) argued that global land areas in drought (defined as bottom 20% of local simulated Palmer Drought Severity Index, PDSI) varied between 14-16% from 1950 to 1982 when a sudden increase of approximately 10% occurred. Thereafter, an upward trend for the spatial extent of areas in drought was demonstrated in Dai (2011) . While our results concur with the fraction of areas in drought and the increase for the global areas under drought around 1982-1983, we only observed a significant increasing trend for land in the SH in moderate to severe ($-2 < \text{SPI} \leq -1$) drought conditions. No significant trends have been observed for the remaining land areas (e.g., land in the NH) - see the third column in Table 5. It should be noted that the results presented in this paper cannot be directly compared with those in Dai (2011) as: (a) the presented results are based on meteorological drought (SPI), while the results in Dai (2011) are based on PDSI; (b) different climatology and data records are used than those in Dai (2011); (c) different thresholds of droughts are used in the two studies; and (d) the presented results are data driven and model independent, while results in Dai (2011) are based on model simulations. Although the results cannot be compared directly, our findings generally agree

with the results presented in Dai (2011).

### 5.1.3 Drying and Wetting Trends on Global scale

Finally, the Mann-Kendall test is performed in pixel-scale to detect drying and wetting trends and their occurrence over the globe. Figure 13 shows a global map of areas with drying, wetting and no trend for the past three decades. Figure 13a and 13b uses the significance level of 0.05 while Figure 13c shows the positive, negative and lack of trends at the significance level of 0.01. The upper panel (Figure 13a) displays the relative S-value (Fatichi, 2009) which is a normalized measure of the cumulative number of positive and negative changes for the pixels in order to express where trends are stronger over the globe.

In Figure 13a, the S-values are normalized from -1 to 1 based on the cumulative number of changes. The closer the S-value is to -1, the stronger the trend of drying is. Conversely, an S-value close to 1, represent a stronger trend for wet conditions. For better visualization, Figure 13 presents the areas with a significant drying trend in red (decreasing SPI over time) and areas with a significant wetting trend in blue (increasing SPI over time). Areas with no significant positive or negative trend appear as white along with areas of perpetual droughts masked out to avoid unreliable statistics according to above. Note that Figure 13b and 13c show the drying (red areas) and wetting (blue areas) trends at 0.05 and 0.01 significance levels, respectively. This indicates higher confidence in the trends provided in Figure 13c.

Figure 13 indicates that several areas such as the southwestern United States, Texas and the Gulf of Mexico region, parts of the Amazon, the Horn of Africa, northern India, and parts of the Mediterranean region are among areas showing a significant drying trend in the past three decades. On the other hand, central Africa, Thailand, Taiwan, central America, northern Australia and parts of eastern Europe show a wetting trend during the same time span. The results of this study are consistent with local studies on droughts in the southwestern United States (Cayan et al., 2010) and Amazon (Marengo et al., 2008); (Marengo et al., 2011).

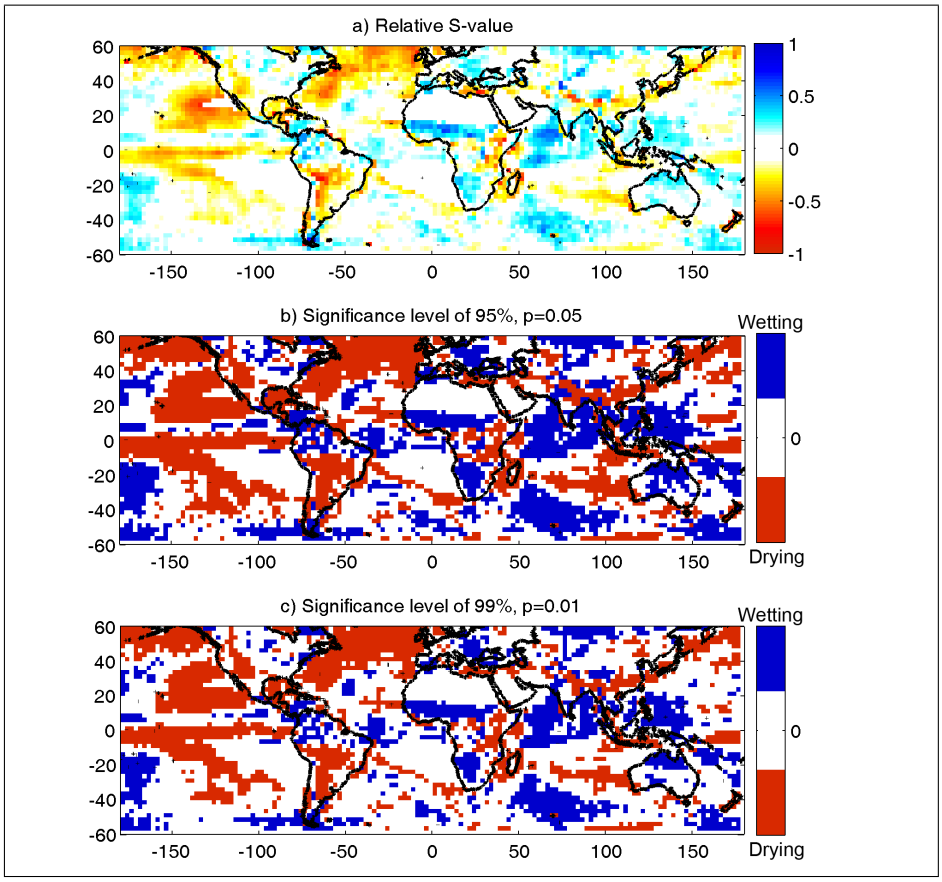


**Figure 13:** a) Global trends of drying and wetting 6-month SPI over the last 32 years expressed a) as a relative S-value between -1 and 1 where -1 symbolizes the strongest drying trend (decrease in SPI over time) and 1 the strongest wetting trends (increase of SPI over time). White are areas with no trends or masked out due to perpetual drought (precipitation $< 0.5$mm/day) b) areas showing significant drying (red) and wetting (blue) trends at a 0.05 significance level, and c) areas showing significant drying (red) and wetting (blue) trends at a 0.01 significance level.

## 5.2 Results for analysis using CMIP5 Models and CRU observations

### 5.2.1 Area under drought

The areas under drought (SPI $\leq$ -1) for (a) all land areas, (b) land areas in the Northern Hemisphere (NH), and (c) land areas in the Southern Hemisphere (SH) are shown in Figure 14.

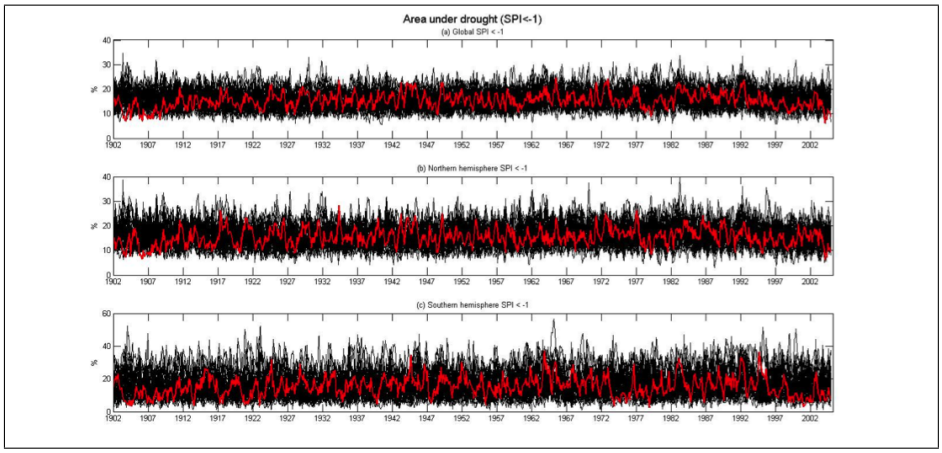


**Figure 14:** Area (%) under drought (SPI $\leq$ -1) from 1902-2004 for: (a) total land areas, (b) land areas in the NH, and (c) land areas in the SH. The black lines represent the 41 CMIP5 climate model simulations, and the red lines indicate CRU data.

The black lines symbolize CMIP5 climate model simulations, and the red line the CRU observations. As shown, the envelope of climate model simulations encompasses the CRU observations at most points. A visual comparison indicates larger variability in SPI values based on CRU observations in the SH than in the NH. Overall, the CMIP5 climate model simulations reconstruct this difference in variability reasonably well. As shown in 14, the range of area under drought in SH varies between 5-50%, while in NH the area under drought never exceeded 40%.

According to the CRU observations, on average ≈15.3% of the land areas have been under drought (SPI $\leq$ -1) during the $20^{th}$ century (see Table 6). The areas under drought in the model simulations range between 15.4% and 16.0%, indicating a reasonable agreement with respect to global averages.

Table 6: Average fraction of area in drought; as a total (SPI $\leq$ -1), extreme droughts separately (SPI $\leq$ -2) and drought for moderate to severe droughts (-1 $\geq$ SPI > -2)

| | **SPI $\leq$ -1** | | | **SPI $\leq$ -2** | | | **-1 $\geq$ SPI > -2** | | |
|---|---|---|---|---|---|---|---|---|---|
| | **Total Land** | **NH** | **SH** | **Total Land** | **NH** | **SH** | **Total Land** | **NH** | **SH** |
| CRU | 15.26 | 15.34 | 15.07 | 2.65 | 2.64 | 2.69 | 12.61 | 12.70 | 12.38 |
| Ensemble mean | 15.81 | 15.90 | 15.61 | 2.29 | 2.24 | 2.42 | 13.52 | 13.65 | 13.19 |
| BCC-CSM1-1 | 15.86 | 15.81 | 15.98 | 2.25 | 2.30 | 2.16 | 13.61 | 13.51 | 13.82 |
| BCC-CSM1-1-esm | 15.93 | 15.95 | 15.89 | 2.20 | 2.25 | 2.11 | 13.73 | 13.70 | 13.78 |

Continued on next page

| | | | | | | | | | |
|---|---|---|---|---|---|---|---|---|---|
| CanESM2 | 15.84 | 15.77 | 15.99 | 2.23 | 2.27 | 2.16 | 13.61 | 13.51 | 13.83 |
| CanESM2-esm | 15.71 | 15.72 | 15.67 | 2.24 | 2.24 | 2.23 | 13.47 | 13.48 | 13.44 |
| CCSM4 | 15.76 | 15.76 | 15.76 | 2.34 | 2.33 | 2.35 | 13.43 | 13.43 | 13.42 |
| CESM1-BGC | 15.85 | 15.87 | 15.80 | 2.27 | 2.29 | 2.25 | 13.58 | 13.59 | 13.56 |
| CESM1-BGC-esm | 15.83 | 15.83 | 15.85 | 2.32 | 2.33 | 2.30 | 13.51 | 13.50 | 13.55 |
| CESM1-CAM5 | 15.82 | 15.84 | 15.78 | 2.27 | 2.24 | 2.34 | 13.55 | 13.59 | 13.44 |
| CESM1-FASTCHEM | 15.87 | 15.87 | 15.88 | 2.28 | 2.27 | 2.30 | 13.59 | 13.60 | 13.58 |
| CESM1-WACCM | 15.82 | 15.83 | 15.80 | 2.43 | 2.36 | 2.62 | 13.38 | 13.47 | 13.18 |
| CNRM-CM5 | 15.83 | 15.81 | 15.89 | 2.15 | 2.22 | 1.99 | 13.68 | 13.59 | 13.90 |
| CSIRO-ACCESS1-0 | 15.86 | 15.91 | 15.75 | 2.41 | 2.48 | 2.24 | 13.46 | 13.44 | 13.51 |
| CSIRO-ACCESS1-3 | 15.93 | 15.89 | 16.02 | 2.38 | 2.36 | 2.42 | 13.55 | 13.54 | 13.60 |
| CSIRO-Mk3-6-0 | 16.00 | 15.92 | 16.20 | 2.42 | 2.44 | 2.37 | 13.57 | 13.47 | 13.83 |
| FGOALS-g2 | 15.96 | 15.92 | 16.05 | 2.26 | 2.29 | 2.21 | 13.70 | 13.63 | 13.84 |
| FGOALS-s2 | 15.77 | 15.82 | 15.65 | 2.44 | 2.38 | 2.57 | 13.33 | 13.44 | 13.09 |
| GFDL-CM3-esm | 15.76 | 15.75 | 15.78 | 2.46 | 2.46 | 2.45 | 13.30 | 13.29 | 13.33 |
| GFDL-ESM2G | 15.82 | 15.89 | 15.66 | 2.66 | 2.64 | 2.73 | 13.16 | 13.25 | 12.93 |
| GFDL-ESM2M | 15.82 | 15.84 | 15.75 | 2.65 | 2.58 | 2.84 | 13.16 | 13.27 | 12.91 |
| GFDL-ESM2M-esm | 15.89 | 15.93 | 15.81 | 2.63 | 2.62 | 2.67 | 13.26 | 13.31 | 13.14 |
| GISS-E2-H | 15.93 | 15.92 | 15.97 | 2.23 | 2.29 | 2.09 | 13.71 | 13.63 | 13.88 |
| GISS-E2-R | 15.99 | 15.99 | 16.00 | 2.17 | 2.24 | 2.00 | 13.82 | 13.75 | 14.00 |
| HadGEM2 | 15.87 | 15.84 | 15.92 | 2.43 | 2.46 | 2.36 | 13.44 | 13.38 | 13.56 |
| HadGEM2-CC | 15.89 | 15.88 | 15.91 | 2.41 | 2.45 | 2.30 | 13.48 | 13.43 | 13.61 |
| HadGEM2-ES-esm | 15.92 | 15.88 | 16.00 | 2.36 | 2.40 | 2.28 | 13.55 | 13.48 | 13.73 |
| INMCM4-esm | 15.91 | 15.93 | 15.88 | 2.35 | 2.44 | 2.13 | 13.57 | 13.49 | 13.75 |
| IPSL-CM5A-LR | 15.90 | 15.83 | 16.07 | 2.44 | 2.48 | 2.36 | 13.46 | 13.36 | 13.71 |
| IPSL-CM5A-LR-esm | 15.96 | 15.99 | 15.89 | 2.43 | 2.41 | 2.48 | 13.53 | 13.58 | 13.41 |
| IPSL-CM5A-MR | 15.81 | 15.83 | 15.75 | 2.41 | 2.45 | 2.29 | 13.40 | 13.37 | 13.46 |
| IPSL-CM5B–LR | 15.77 | 15.81 | 15.69 | 2.31 | 2.28 | 2.40 | 13.46 | 13.53 | 13.29 |
| MIROC5 | 15.85 | 15.89 | 15.75 | 2.36 | 2.32 | 2.46 | 13.49 | 13.57 | 13.28 |
| MIROC-ESM | 15.84 | 15.81 | 15.91 | 2.51 | 2.43 | 2.70 | 13.33 | 13.38 | 13.20 |
| MIROC-ESM-CHEM | 15.85 | 15.82 | 15.92 | 2.53 | 2.47 | 2.68 | 13.32 | 13.35 | 13.25 |
| MIROC-ESM-esm | 15.86 | 15.89 | 15.79 | 2.47 | 2.39 | 2.66 | 13.39 | 13.50 | 13.14 |
| MPI-ESM-LR | 15.82 | 15.84 | 15.76 | 2.68 | 2.62 | 2.84 | 13.14 | 13.23 | 12.92 |
| MPI-ESM-LR-esm | 15.75 | 15.75 | 15.76 | 2.69 | 2.63 | 2.83 | 13.06 | 13.12 | 12.93 |

Continued on next page

| | | | | | | | | | |
|---|---|---|---|---|---|---|---|---|---|
| MPI-ESM-P | 15.76 | 15.90 | 15.44 | 2.61 | 2.54 | 2.77 | 13.15 | 13.36 | 12.67 |
| MRI-CGCM3 | 15.98 | 15.98 | 15.98 | 2.29 | 2.34 | 2.17 | 13.69 | 13.64 | 13.81 |
| MRI-ESM1 | 15.93 | 15.90 | 16.00 | 2.33 | 2.41 | 2.16 | 13.60 | 13.49 | 13.85 |
| NorESM1-M | 15.86 | 15.84 | 15.91 | 2.40 | 2.40 | 2.40 | 13.46 | 13.44 | 13.51 |
| NorESM1-ME | 15.84 | 15.83 | 15.88 | 2.42 | 2.38 | 2.50 | 13.42 | 13.44 | 13.38 |

The global averages of area under drought during the last century correspond reasonably well with previous studies by Sheffield and Wood (2008) and Dai (2012) who determined the average area of lands under drought to be 20%, and 14-20%, respectively. However, as was the case with the satellite based results, neither can those results be compared directly as the findings of Sheffield and Wood (2008) and Dai (2012) are based on different climatologies, time scales and indicator variables. Figure 15 presents areas under extreme drought (SPI $\leq$ 2) for (a) all land areas, (b) land areas in the NH, and (c) land areas in the SH. As shown in both Figures 14, and 15, at several time points, climate model simulations substantially overestimate areas under drought.

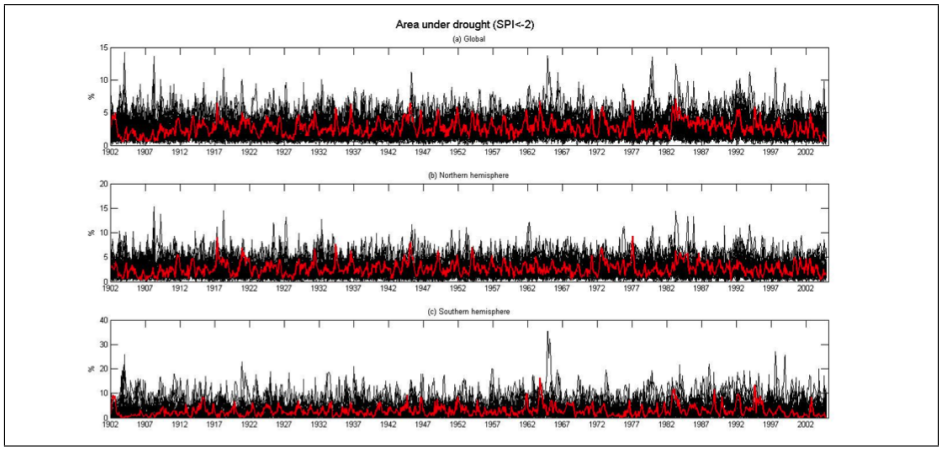


**Figure 15:** Area (%) under extreme drought conditions (SPI $\leq$ -2) from 1902-2005 for: (a) total land areas, (b) land areas in the NH, and (c) land areas in the SH. Black lines represent the 41 models, and the red lines indicate CRU data.

From Figure 15, the CMIP5 multi-model simulations encompass the observations at most (but not all) time steps during the period of 1902-2005, and the CMIP5 simulations substantially overestimate the area in extreme drought (SPI $\leq$ -2) in the SH where the variability is generally larger (the area under extreme droughts in the NH is never greater than 15%, while in SH it exceeds 25% at several time points). Nevertheless, on average $\approx$ 2.7% of the global land area in both simulations and observations is subject to extreme drought.

### 5.2.2 Trends in Area under Drought

It is found that the CRU observational time serie of area under drought shows a significant positive trend for all land areas, both NH and SH, at a significance level of 0.05 (see H-values reported in Table 7). This situation is reproduced by 30 (73%) of the 41 CMIP5 models, but not by their ensemble mean. When considering the NH and the SH separately, 29 (71%) and 27 (66%) of the CMIP5 climate models confirm the observed significant trends (Table 7, columns 2 and 3, respectively). Thus, overall the results indicate that a large majority of the CMIP5 model agree with observations with respect to global and hemispheric trends. It should be noted that the model simulations in Table 1 that are designated as "esm" (historical simulations of climate with atmospheric $CO_2$ emissions specified in coupled earth systems models (ESMs) with a prognostic carbon cycle) do not exhibit a systematic pattern relative to the rest of the model simulations in which the historical time series of global atmospheric $CO_2$ concentrations are prescribed. That is, "esm" models are not systematically better/worse in detecting drought trends relative to the other models.

Table 7: H-values from the Mann-Kendall statistical significance test for areas in drought (SPI < -1) over global land areas ("Land"), and of those in only the Northern Hemisphere (NH) and in the Southern Hemisphere (SH). The detection of a significant trend is indicated by "1", and no significant trend by a "0").

| | **p=0.05** | | | | **p=0.01** | | | |
|---|---|---|---|---|---|---|---|---|
| | **Total Land** | **NH** | **SH** | **POD** | **Total Land** | **NH** | **SH** | **POD** |
| CRU | 1 | 1 | 1 | 1 | 1 | 1 | 1 | 1 |
| Ensemble mean | 0 | 1 | 1 | 0.362 | 0 | 1 | 1 | 0.354 |
| BCC-CSM1-1 | 0 | 1 | 1 | 0.396 | 0 | 1 | 1 | 0.434 |
| BCC-CSM1-1-esm | 0 | 0 | 0 | 0.432 | 0 | 0 | 0 | 0.459 |
| CanESM2 | 1 | 1 | 1 | 0.385 | 1 | 1 | 1 | 0.436 |
| CanESM2-esm | 1 | 0 | 1 | 0.416 | 0 | 0 | 0 | 0.456 |
| CCSM4 | 1 | 1 | 1 | 0.422 | 1 | 0 | 1 | 0.454 |
| CESM1-BGC | 1 | 1 | 1 | 0.4 | 1 | 1 | 1 | 0.44 |
| CESM1-BGC-esm | 0 | 0 | 0 | 0.407 | 0 | 0 | 0 | 0.45 |
| CESM1-CAM5 | 1 | 1 | 1 | 0.379 | 1 | 1 | 1 | 0.395 |
| CESM1-FASTCHEM | 1 | 1 | 0 | 0.434 | 1 | 1 | 0 | 0.45 |
| CESM1-WACCM | 1 | 1 | 0 | 0.413 | 1 | 1 | 0 | 0.443 |

Continued on next page

| | | | | | | | | |
|---|---|---|---|---|---|---|---|---|
| CNRM-CM5 | 0 | 1 | 1 | 0.386 | 0 | 0 | 1 | 0.423 |
| CSIRO-ACCESS1-0 | 1 | 1 | 1 | 0.357 | 1 | 1 | 0 | 0.385 |
| CSIRO-ACCESS1-3 | 1 | 1 | 0 | 0.403 | 0 | 1 | 0 | 0.418 |
| CSIRO-Mk3-6-0 | 0 | 1 | 0 | 0.348 | 0 | 1 | 0 | 0.384 |
| FGOALS-g2 | 1 | 1 | 1 | 0.398 | 1 | 1 | 1 | 0.447 |
| FGOALS-s2 | 1 | 1 | 1 | 0.423 | 1 | 1 | 1 | 0.424 |
| GFDL-CM3-esm | 1 | 1 | 1 | 0.401 | 1 | 1 | 0 | 0.435 |
| GFDL-ESM2G | 0 | 0 | 0 | 0.416 | 0 | 0 | 0 | 0.463 |
| GFDL-ESM2M | 0 | 0 | 0 | 0.456 | 0 | 0 | 0 | 0.495 |
| GFDL-ESM2M-esm | 0 | 0 | 0 | 0.423 | 0 | 0 | 0 | 0.455 |
| GISS-E2-H | 1 | 1 | 1 | 0.324 | 1 | 1 | 1 | 0.33 |
| GISS-E2-R | 1 | 0 | 1 | 0.348 | 1 | 0 | 1 | 0.354 |
| HadGEM2 | 1 | 1 | 1 | 0.366 | 1 | 1 | 1 | 0.378 |
| HadGEM2-CC | 1 | 1 | 1 | 0.316 | 1 | 1 | 1 | 0.354 |
| HadGEM2-ES-esm | 1 | 1 | 1 | 0.357 | 1 | 1 | 1 | 0.378 |
| INMCM4-esm | 1 | 0 | 1 | 0.39 | 1 | 0 | 1 | 0.426 |
| IPSL-CM5A-LR | 1 | 1 | 0 | 0.409 | 1 | 0 | 0 | 0.429 |
| IPSL-CM5A-LR-esm | 0 | 1 | 0 | 0.433 | 0 | 0 | 0 | 0.452 |
| IPSL-CM5A-MR | 1 | 1 | 1 | 0.394 | 1 | 1 | 0 | 0.431 |
| IPSL-CM5B-LR | 1 | 1 | 1 | 0.427 | 1 | 1 | 1 | 0.454 |
| MIROC5 | 1 | 1 | 1 | 0.416 | 1 | 1 | 1 | 0.432 |
| MIROC-ESM | 1 | 1 | 0 | 0.397 | 1 | 1 | 0 | 0.423 |
| MIROC-ESM-CHEM | 1 | 1 | 0 | 0.395 | 1 | 1 | 0 | 0.421 |
| MIROC-ESM-esm | 1 | 1 | 1 | 0.396 | 1 | 1 | 1 | 0.405 |
| MPI-ESM-LR | 1 | 1 | 1 | 0.322 | 0 | 1 | 1 | 0.351 |
| MPI-ESM-LR-esm | 0 | 1 | 1 | 0.323 | 0 | 1 | 1 | 0.338 |
| MPI-ESM-P | 1 | 0 | 1 | 0.329 | 1 | 0 | 1 | 0.338 |
| MRI-CGCM3 | 1 | 0 | 1 | 0.414 | 1 | 0 | 1 | 0.441 |
| MRI-ESM1 | 1 | 0 | 1 | 0.39 | 1 | 0 | 1 | 0.403 |
| NorESM1-M | 0 | 1 | 0 | 0.402 | 0 | 1 | 0 | 0.446 |
| NorESM1-ME | 1 | 0 | 1 | 0.374 | 1 | 0 | 1 | 0.405 |

### 5.2.3 Drying and Wetting Trends on Global scale

In order to investigate the spatial pattern of droughts, the wetting and drying trends are investigated at pixel-scale. Figure 16 presents significant drying (red) and wetting (blue) trends based on CRU observations and a subset of CMIP5 simulations (significance level: 0.05).

In Figure 16, observations exhibit a significant drying trend in the northeas-

tern India, and in scattered areas over Europe and the United States. As shown, most CMIP5 models are in rough agreement with the observed trends here, although the exact locations and spatial extents are not necessarily consistent with the observations. Figure 16 also show that, based on CRU observations, there are areas with significant wetting trends over high latitudes (i.e., northern Canada, Europe and Russia). Collectively, CMIP5 climate models are in better agreement with observations over high latitudes. On the other hand, there are areas where observations and almost all models disagree, such as southeastern China, and regions of South America, South Africa and Australia.

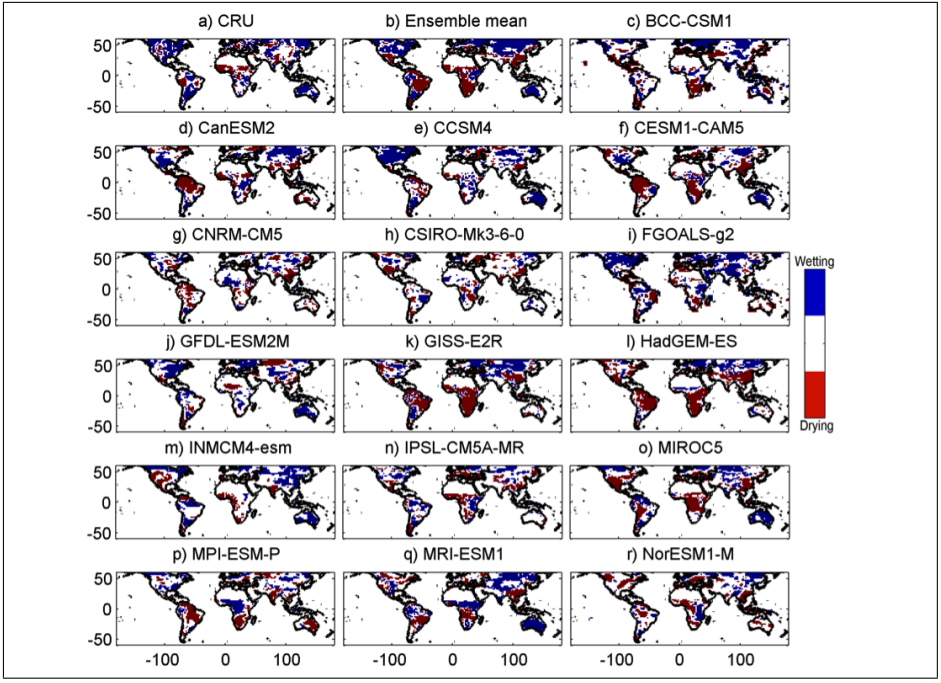


**Figure 16:** Wetting and drying trends from the Mann-Kendall test performed pixel-by-pixel for the last 102 years. The blue areas show wetting trends, and the red areas indicate drying trends at a significance level of 0.05.

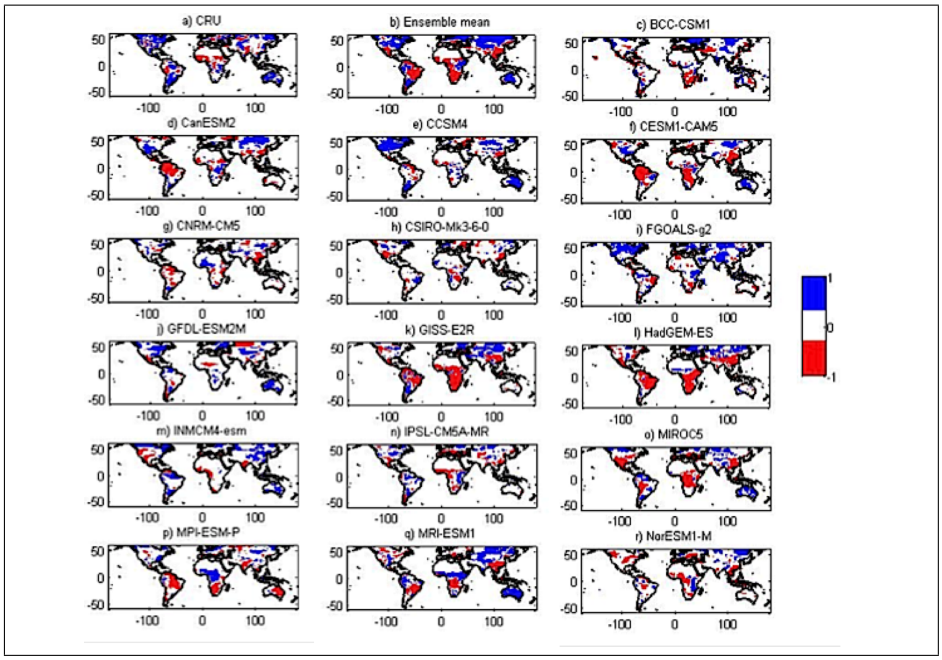


**Figure 17:** Wetting and drying trends from the Mann-Kendall test performed pixel-by-pixel for the last 102 years. The blue areas show wetting trends, and the red areas indicate drying trends at a significance level of 0.01.

In Figure 17, wetting and drying trends at a significance level of 0.01are presented. There are less areas displaying significant trends as a total, and while the observations show an almost unchanged area of drying trends for the part of the southwestern US and northern India mentioned, many models show decreasing areas in these regions.

### 5.2.4 Probability of Detection of Drying and Wetting trends

In order to quantitatively assess the ability of the model to identify the location of wetting/drying trends, the Probability of Detecting (POD) trends correctly is computed for all models and listed in Table 7. Here, the POD is defined as the ratio of land pixels where the trends (whether positive/negative/no trend) are identified correctly divided by the total number of land pixels. In other words, the POD statistic only measures agreement in the sign of a significant trend, not in its magnitude. The POD values (at significance level of p=0.05) range between 0.32 and 0.46 (average ≈0.40), indicating that on average CMIP5 models identify trends similar to those of observations over about 40% of land areas.

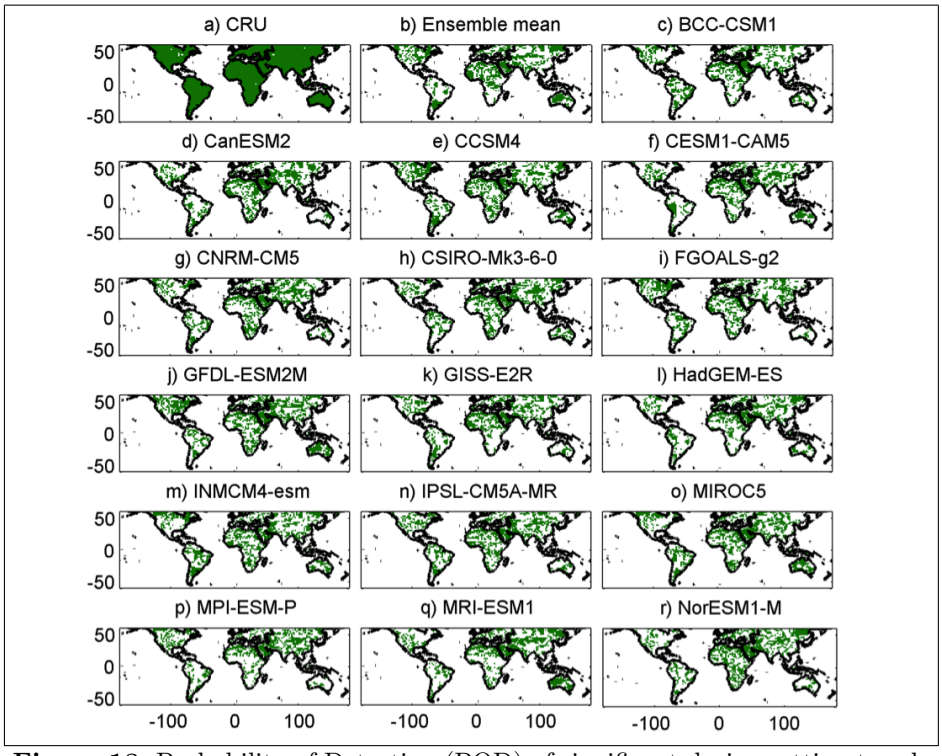


**Figure 18:** Probability of Detection (POD) of significant dryingwetting trends or lack of a trend at significance level p=0.05. Green (white) pixels indicate the simulations were consistent (inconsistent) with CRU observations with regard to the drought trends.

Figure 18 displays areas where CMIP5 climate model simulations match CRU observations with respect to sign of the trend. In the figure, the green pixels indicate matches between the trends in observations and CMIP5 simulations, whereas white (colorless) pixels show areas where models simulations and observations are inconsistent in terms of trends. One can see that the ensemble mean (Figure 18b) is not necessarily superior to individual CMIP5 climate models.

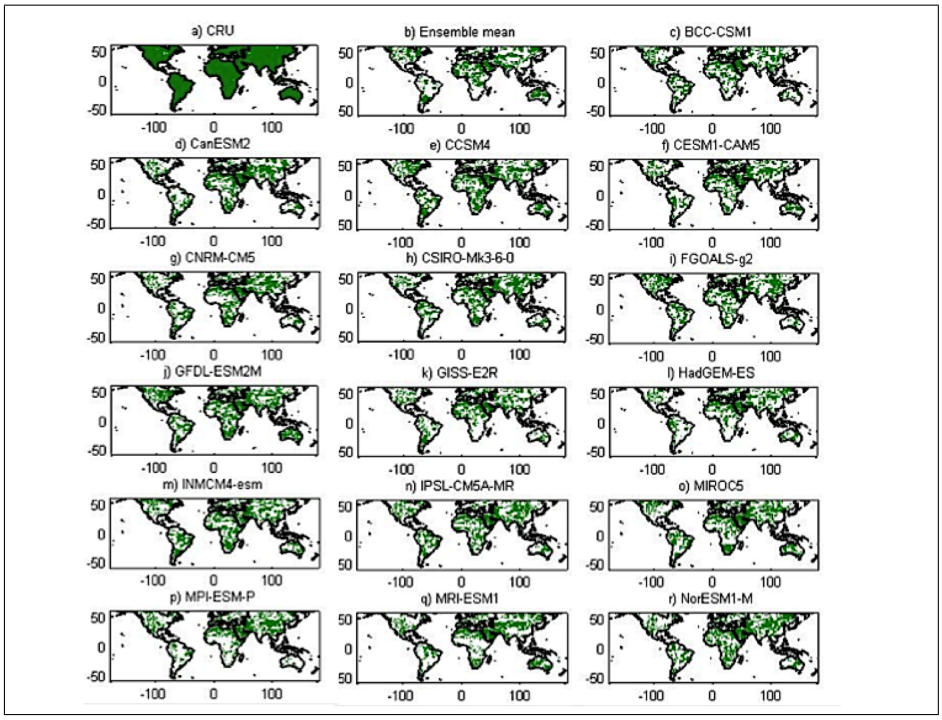


**Figure 19:** Probability of Detection (POD) of significant dryingwetting trends or lack of a trend at significance level of 0.01. Green (white) pixels indicate the simulations were consistent (inconsistent) with CRU observations with regard to the drought trends.

For the significance level of 0.01(see Figure 19), the models show matching trends in 0.34 -0.49 (0.42 as an average) of the pixels over land. A reason for the improved performance at a higher significance level can be the increase in pixels showing no trend for both models and observations. Apart from the increased fraction of matching pixels, similar patterns are shown between the two significance levels (p = 0.05 and P= 0.01).

# 6 Conclusions

Numerous studies argue that the climate is changing rapidly especially since the second half of the twentieth century (Trenberth, 2001). The acceleration of the hydrologic cycle (Trenberth, 1999) indicates that certain regions may become drier while other areas may become wetter. In fact, an increase or decrease in temperature would alter precipitation patterns and frequency, and thus intensity and occurrence of droughts. Given the significance of understanding past changes in droughts and their frequency of occurrence to predict future droughts, this thesis analyzes spatial patterns and trends in two different semi-global precipitation records, the first one a merged satellite-based product spanning from

1979 to present time and the second a multimodel ensemble from CMIP5 where the main objective was to investigate similarities between observations and simulations. Initially, conclusions are given for each study separately and thereafter followed by overall conclusions and comments on future work.

## 6.1 Analysis based on Satellite Data

In the first part of the thesis the aim was to investigate a recently presented model-independent data set. Results from the satellite-based study show on average 15 to 16% of the globe is under drought (SPI $\leq$ -1) from which 2 to 3% is in an extreme drought condition. The analysis demonstrates that droughts in terms of both amplitude and frequency are more variable over land in the SH than in the NH - see Figures 11a and 11b. Unlike land, droughts over the ocean in the NH and the SH are more consistent with respect to their area which is approximately 15 to 16% of respective ocean area. The variability (range of change) for the fraction of land in moderate to severe drought conditions (-2 $<$ SPI $\leq$ -1) is approximately 19% in the NH, while it is over 30% in the SH. This indicates that in terms of both amplitude and frequency, land droughts are more variable in the SH than in the NH.

In addition to these overall results, the results of the Mann-Kendall test reveal that the area under drought increases over the entire globe and over the oceans, but not over land (see Table 5). However, after investigating land in the NH and SH separately, the results exhibit a significant positive trend in the land area under drought in the SH, while no significant trend is observed over land in the NH.

From the analysis of spatial patterns of wetting and drying trends maps were created from the pixel-based satellite data. The maps show that several regions, such as the southwestern United States exhibit a significant trend of drought severity. Other areas, such as the Gulf of Mexico region, Texas, parts of the Amazon, the Horn of Africa, northern India, and parts of the Mediterranean region also show a significant drying trend during the past three decades. The global trend maps indicate that central Africa, parts of southwest Asia (e.g., Thailand, Taiwan), central America, northern Australia and parts of eastern Europe show a wetting trend. The results of this study are consistent with various previous studies showing an increase in droughts for the areas with drying trends.

In conclusion, one objective of this part of the thesis was to investigate droughts independent of climate models and based on spatial observations. Overall, the results of this satellite-based study agree with several model-based studies (e.g., (Dai, 2012)) that indicate droughts have been increasing global-

ly, however the lack of trend over land areas may correspond to the recently published article on overestimated historical droughts by Sheffield et al. (2012). The authors stress the importance of using independent data sets to cross-validate climate model simulations. Given that satellite-based climate data records are emerging, we expect that in near future more research will be devoted to investigating spatial patterns of climate extremes.

## 6.2 Analysis based on CMIP5 simulations

Assessing the uncertainties and understanding the deficiencies of climate models is fundamental to developing adaptation strategies (e.g. (Brekke and Barsugli, 2012) and (AghaKouchak et al., 2012)). The objective of this part of the study is to understand how well CMIP5 climate model simulations replicate ground-based observations of the areas under drought, as well as significant wetting/drying trends, and their associated across the globe.

The results showed that the CMIP5 multi-model ensemble encompasses the Climate Research Unit ground-based observations of area under drought at most-steps. Overall, the CMIP5 global averages of area under drought during the last century correspond well with CRU observations and previous studies. However, considering the ensemble of CMIP5 simulations, most members overestimate the areas under extreme drought, particularly in SH. Furthermore, the results showed that the time series of observations and CMIP5 simulations of areas under drought exhibit more variability in SH compared to NH.

The trend analysis of areas under drought revealed that the observational data exhibit a positive trend at the significance level of 0.05 over all land areas, and in the NH and the SH as well. This situation is reconstructed by 73% of the CMIP5 models when looking at total land areas in drought. Over the NH and SH respectively, 71% and 66% of the CMIP5 climate models are consistent with CRU observations with regard to the drought trends. This indicates that most CMIP5 models agree with observations with respect to global trends.

While the global model simulations were generally consistent with observations at a global or hemispheric scale, most do not agree with respect to observed regional drying and wetting trends. Over many regions such as southeastern China, and parts of South America and Africa, the CMIP5 simulations are not consistent with one another or with the observed trends. On the other hand, CMIP5 simulations of regional trends are collectively in better agreement with observations over high latitudes, as well as northeastern India and the western United States.

A probability of detection (POD) test was used to assess the ability of the CMIP5 climate models to identify the location of wetting/drying trends quan-

titatively, it is found that the CMIP5 simulations correctly identify such trends over only about 40% of land areas, on average. The results indicated that while the global and hemispheric trends in most CMIP5 climate models are collectively consistent with observations, one cannot expect these models to adequately reproduce observed trends at regional scales.

## 6.3 Conclusions and Future Work

The main motivation for efforts to simulate the future climate is to provide a better understanding of anticipated changes to the Earth system and climate variables. Assessing the uncertainties and understanding the deficiencies of climate models is fundamental to developing adaptation strategies (e.g., (Brekke and Barsugli, 2012) ; (AghaKouchak et al., 2012)). We stress the importance of using independent data sets to cross-validate climate model simulations. Given that satellite-based climate data records are emerging, we expect that in near future more research will be devoted to investigating spatial patterns of climate extremes.

For this thesis, the results are generated by similar methodology but using different precipitation records. As the length of time series differ greatly comparisons are futile between the two parts of the study. However, one conclusion indicated in both studies is the higher variability of the SH than the NH. Furthermore, both studies show some similar patterns with earlier studies, both model and observation based. The importance of evaluation and validation of datasets is crucial and as the satellite-based data set agree with earlier results, satellite data show promise to become useful in validation of climate model simulations. Therefore, a continued research effort, on both improving climate models as well as satellite products are essential to improve drought monitoring and predictions in the future.

For future studies it would be interesting to analyze the CMIP5 simulations for the last three decades and compare with the satellite based merged dataset. For both datasets, in-depth studies on how well the data set captures changes in patterns and trends at a regional levels would be interesting. Other fields to look into would be the performance over; various climate regions; different latitudes or over urban/rural areas. The satellite data also gives an interesting opportunity to investigate the precipitation patterns over ocean areas more in depth, which has not been possible previously due to lack of information. In the future, an extension of the satellite based dataset to incorporate seasonal (6-9 months) drought forecasts for comparison with model forecasts, would be of interest. Finally, connecting the results with the field of responsible dynamics, not addressed in this thesis, could also provide interesting results.

# References


R. Adler, G. Huffman, A. Chang, R. Ferraro, P. Xie, J. Janowiak, B. Rudolf, U. Schneider, S. Curtis, D. Bolvin, A. Gruber, J. Susskind, and P. Arkin. The version-2 global precipitation climatology project (gpcp) monthly precipitation analysis (1979 - present). *Journal of Hydrometeorology*, 4:1147–1167, 2003.

A. AghaKouchak and N. Nakhjiri. A Near Real-Time Satellite-Based Global Drought Climate Data Record. *Environmental Research Letters*, 7(4), 2012.

A. AghaKouchak, N. Nasrollahi, J. Li, B. Imam, and S. Sorooshian. Geometrical characterization of precipitation patterns. *Journal of Hydrometeorology*, 12 (2):274–285, 2011.

A. AghaKouchak, D. Easterling, K. Hsu, S. Schubert, and S. Sorooshian. *Extremes in a Changing Climate: Detection, Analysis and Uncertainty*. Springer, 2012. ISBN 978-94-007-4478-3.

A. AghaKouchak, A. Behrangi, S. Sorooshian, K. Hsu, and E. Amitai. Evaluation of satellite-retrieved extreme precipitation rates across the central United States. *Journal of Geophysical Research-Atmospheres*, 116, 2011.

L. Alexander and J. Arblaster. Assessing trends in observed and modelled climate extremes over australia in relation to future projections. *International Journal of Climatology*, 29(3):417–435, 2009.

M. C. Anderson, C. Hain, B. Wardlow, A. Pimstein, J. R. Mecikalski, and W. P. Kustas. Evaluation of Drought Indices Based on Thermal Remote Sensing of Evapotranspiration over the Continental United States. *Journal of Climate*, 24(8):2025–2044, 2011.

K. Andreadis, E. Clark, A. Wood, A. Hamlet, and D. Lettenmaier. Twentieth-century drought in the conterminous United States. *Journal of Hydrometeorology*, 6(6):985–1001, DEC 2005. ISSN 1525-755X. doi: {10.1175/JHM450.1}.

K. M. Andreadis, E. A. Clark, D. P. Lettenmaier, and D. E. Alsdorf. Prospects for river discharge and depth estimation through assimilation of swath-altimetry into a raster-based hydrodynamics model. *Geophysical Research Letters*, 34(10), 2007. doi: {10.1029/2007GL029721}.

A. Behrangi, B. Khakbaz, T. Jaw, A. AghaKouchak, K. Hsu, and S. Sorooshian. Hydrologic evaluation of satellite precipitation products at basin scale. *Journal of Hydrology*, 397:225–237, 2011.

L. Brekke and J. Barsugli. Uncertainties in projections of future changes in extremes. In A. AghaKouchak, D. Easterling, K. Hsu, S. Schubert, and S. Sorooshian, editors, *Extremes in a Changing Climate: Detection, Analysis and Uncertainty*. Springer, 2012. DOI: 10.1007/978-94-007-4479-0 11.

J. F. Brown, B. D. Wardlow, T. Tadesse, M. J. Hayes, and B. C. Reed. The Vegetation Drought Response Index (VegDRI): A new integrated approach for monitoring drought stress in vegetation. *Giscience & Remote Sensing*, 45 (1):16–46, 2008.

D. R. Cayan, T. Das, D. W. Pierce, T. P. Barnett, M. Tyree, and A. Gershunov. Future dryness in the southwest US and the hydrology of the early 21st century drought. *Proceedings of the National Academy of Sciences of the United States of America*, 107(50):21271–21276, DEC 14 2010. ISSN 0027-8424. doi: {10.1073/pnas.0912391107}.

Center for Hydrometeorology and Remote Sensing. Precipitation estimation from satellite data, 2004. URL `http://chrs.web.uci.edu/research/satellite_precipitation/approach.html#training`.

C. A. S. Coelho and L. Goddard. El Nino-Induced Tropical Droughts in Climate Change Projections. *Journal of Climate*, 22(23):6456–6476, DEC 1 2009. ISSN 0894-8755. doi: {10.1175/2009JCLI3185.1}.

A. Dai. Drought under global warming: a review. *Wiley Interdisciplinary Reviews-Climate Change*, 2(1):45–65, JAN-FEB 2011. ISSN 1757-7780. doi: {10.1002/wcc.81}.

A. Dai. Increasing drought under global warming in observations and models. *Nature Climate Change*, 2:doi:10.1038/nclimate1633, 2012. doi: {doi:10.1038/nclimate1633}.

A. Dai, K. Trenberth, and T. Qian. A global dataset of Palmer Drought Severity Index for 1870-2002: Relationship with soil moisture and effects of surface warming. *Journal Of Hydrometeorology*, 5(6):1117–1130, 2004. doi: {10.1175/JHM-386.1}.

P. Dirmeyer, X. Gao, Z. Gao, T. Oki, and M. Hanasaki. The global soil wetness project (gswp-2). *Bull. Amer. Meteo. Soc.*, 87:1381–1397, 2006.

D. Easterling. Global data sets for analysis of climate extremes. In A. AghaKouchak, D. Easterling, K. Hsu, S. Schubert, and S. Sorooshian, editors, *Extremes in a Changing Climate: Detection, Analysis and Uncertainty*. Springer, 2012. DOI: 10.1007/978-94-007-4479-0 12.

D. C. Edwards. Charateristics of 20th Century Drought in the United States at Multiple Time Scales. Master's thesis, Colorado State University, Fort Collins, Colorado, 1997.

European Drought Observatory. Fapar anomaly: Anomaly of fraction of absorbed photosynthetically active radiation. http://edo.jrc.ec.europa.eu/documents/factsheets/factsheet_fapar.pdf, 2012.

J. S. Famiglietti, M. Lo, S. L. Ho, J. Bethune, K. J. Anderson, T. H. Syed, S. C. Swenson, C. R. de Linage, and M. Rodell. Satellites measure recent rates of groundwater depletion in california's central valley. *Geophysical Research Letters*, 38(3):n/a–n/a, 2011. ISSN 1944-8007. doi: 10.1029/2010GL046442. URL `http://dx.doi.org/10.1029/2010GL046442`.

S. Fatichi. Mann-kendall test. Technical report, Dipartimento Ingegneria Civile e Ambientale, Universita degli Studi di Firenze, 2009. URL `http://www.mathworks.com/matlabcentral/fileexchange/25531-mann-kendall-test`.

A. K. Fleig, L. M. Tallaksen, H. Hisdal, and S. Demuth. A global evaluation of streamflow drought characteristics. *Fydrological Earth System Scinces Discussions*, 10:535–552, 2006.

P. Frich, L. Alexander, P. Della-Marta, B. Gleason, M. Haylock, A. Klein Tank, and T. Peterson. Observed coherent changes in climatic extremes during the second half of the twentieth century. *Climate Research*, 19:193–212, 2002.

Global Runoff Data Center. Global runoff data center. http://www.bafg.de/, 2008.

Y. Gu, E. Hunt, B. Wardlow, J. B. Basara, J. F. Brown, and J. P. Verdin. Evaluation of modis ndvi and ndwi for vegetation drought monitoring using oklahoma mesonet soil moisture data. *Geophysical Research Letters*, 35(L22401), 2008.

Z. Hao and A. AghaKouchak. A multivariate multi-index drought modeling framework. *Journal of Hydrometeorology*, -(-):–, 2012. under review.

M. Hayes. *Climate Change in the Midwest: Impacts, Risks, Vulnerability, and Adaptation*, chapter 13. Indiana University Press, 2012.

M. Hayes, M. Svoboda, D. Wilhite, and O. Vanyarkho. Monitoring the 1996 drought using the standardized precipitation index. *Bull. Amer. Meteor.Soc.*, 80:429–438, 1999.

M. Hayes, M. Svoboda, N. Wall, and M. Widhalm. The lincoln declaration on drought indices: Universal meteorological drought index recommended. *Bulletin of the American Meteorological Society*, 92(4):485–488, 2011.

R. Heim. A review of twentieth-century drought indices used in the United States. *Bulletin Of The American Meteorological Society*, 83(8):1149–1165, 2002.

D. Helsel and R. Hirsh. Trend analysis. Technical report, In D.R. Helsel, and R.M. Hirsh, Statistical Methods in Water Resources. U S Geological Survey, 2010.

R. Hirsch and J. E. Costa. U.s. stream flow measurement and data dissemination improve. *Eos Transactions - AGU Fall Meet. Suppl.*, 85(20), 2004.

K. Hsu, X. Gao, S. Sorooshian, and H. Gupta. Precipitation estimation from remotely sensed information using artificial neural networks. *Journal of Applied Meteorology*, 36:1176ñ1190, 1997.

G. Huffman, R. Adler, D. Bolvin, G. Gu, E. Nelkin, K. Bowman, E. Stocker, and D. Wolff. The trmm multi-satellite precipitation analysis: Quasi-global, multiyear, combined-sensor precipitation estimates at fine scale. *J. Hydrometeorol.*, 8:38ñ55, 2007.

G. J. Huffman, R. F. Adler, D. T. Bolvin, and G. Gu. Improving the global precipitation record: GPCP Version 2.1. *Geophysical Research Letters*, 36, SEP 10 2009. ISSN 0094-8276. doi: {10.1029/2009GL040000}.

T. G. Huntington. Evidence for intensification of the global water cycle: Review and synthesis. *Journal of Hydrology*, 319(1ââĆň“4):83 – 95, 2006. ISSN 0022-1694. doi: 10.1016/j.jhydrol.2005.07.003. URL `http://www.sciencedirect.com/science/article/pii/S0022169405003215`.

IPCC. *Managing the Risks of Extreme Events and Disasters to Advance Climate Change Adaptation Special Report of the Managing the Risks of Extreme Events and Disasters to Advance Climate Change Adaptation: Special Report of the Intergovermental Panel on CLimate Change*. Working Groups I and II of the Intergovernmental Panel on Climate Change, 2012.

R. Joyce, J. Janowiak, P. Arkin, and P. Xie. Cmorph: A method that produces global precipitation estimates from passive microwave and infrared data at high spatial and temporal resolution. *J. Hydrometeorol.*, 5:487ñ 503, 2004.

T. R. Karl. The sensitivity of the palmer drought severity index and palmer's z-index to their calibration coefficients including potential evapotranspiration.

*Journal of Climate and Applied Meteorology*, 25(1):77–86, 2013/01/07 1986. doi: 10.1175/1520-0450(1986)025<0077:TSOTPD>2.0.CO;2. URL `http://dx.doi.org/10.1175/1520-0450(1986)025<0077:TSOTPD>2.0.CO;2`.

M. Kendall. *Rank Correlation Methods*. 4th Ed. Griffin, 1976.

D. G. C. Kirono and D. M. Kent. Assessment of rainfall and potential evaporation from global climate models and its implications for Australian regional drought projection. *International Journal of Climatology*, 31(9):1295–1308, JUL 2011. ISSN 0899-8418. doi: {10.1002/joc.2165}.

H. Lau, K. M.; Weng. Teleconnection linking asian/pacific monsoon variability and summertime droughts and floods over the united states. Technical Report GCN-00-09 20000060826, NASA Goddard Space Flight Center, March 2000.

T. Lee. Standard precipitation index. Technical report, Institut National de la Recherche Scintifique - Eau Terre Environment (INRS-ETE), Quebec, Canada, Dec 2009.

H. Mann. Nonparametric tests against trend. *Econometrica*, 13:245–259, 1945.

J. A. Marengo, C. A. Nobre, J. Tomasella, M. D. Oyama, G. S. De Oliveira, R. De Oliveira, H. Camargo, L. M. Alves, and I. F. Brown. The drought of Amazonia in 2005. *Journal of Climate*, 21(3):495–516, FEB 2008. ISSN 0894-8755. doi: {10.1175/2007JCLI1600.1}.

J. A. Marengo, J. Tomasella, L. M. Alves, W. R. Soares, and D. A. Rodriguez. The drought of 2010 in the context of historical droughts in the Amazon region. *Geophysical Research Letters*, 38, JUN 22 2011. doi: {10.1029/2011GL047436}.

T. McKee, N. Doesken, and J. Kleist. The relationship of drought frequency and duration to time scales. In *In Proceedings of the 8th Conference of Applied Climatology, 17-22 January 1993. Anaheim, CA, American Meteorological Society*, pages 179–184, 1993.

G. Meehl and S. Bony. Introduction to CMIP5. *Clivar Exchanges*, 16(2):4–5, 2011.

P. Milly, K. A. Dunne, and A. V. Vecchia. Global pattern of trends in streamflow and water availability in a changing climate. *Nature*, 2005.

A. K. Mishra and V. P. Singh. A review of drought concepts. *Journal of Hydrology*, 391(1-2):204–216, 2010.

T. Mitchell and P. Jones. An improved method of constructing a database of monthly climate observations and associated high-resolution grids. *International Journal of Climatology*, 25(6):693–712, 2005.

K. Mo. Model based drought indices over the United States. *Journal of Hydrometeorology*, 9:1212–1230, 2008.

N. Nakhjiri. New standardized precipitation index. Matlab code, available, 2012.

T. Oki and S. Kanae. Global hydrological cycles and world water resources. *Science*, 313:1068 – 1072, August 2006.

W. Palmer. Meteorological drought. Technical report, Weather Bureau Res. Paper 45, U.S. Dept. of Commerce, 1965. 58 pp.

F. Panagiotopoulos, M. Shahgedanova, and D. B. Stephenson. A review of northern hemisphere winter-time teleconnection patterns. *J. Phys. IV France*, 12(10):27–47, 11 2002. URL `http://dx.doi.org/10.1051/jp4:20020450`.

M. C. Peel, B. L. Finlayson, and T. A. McMahon. Updated world map of the köppen-geiger climate classification. *Hydrology and Earth System Sciences*, 11(5):1633–1644, 2007.

B. Rajagopalan, E. Cook, U. Lall, and B. K. Ray. Spatiotemporal variability of enso and sst teleconnections to summer drought over the united states during the twentieth century. *Journal of Climate*, 13(24):4244–4255, 2013/01/06 2000. doi: 10.1175/1520. URL `http://dx.doi.org/`.

Y. Richard, N. Fauchereau, I. Poccard, M. Rouault, and S. Trzaska. 20th century droughts in southern africa: spatial and temporal variability, teleconnections with oceanic and atmospheric conditions. *International Journal of Climatology*, 21(7):873–885, 2001. ISSN 1097-0088. doi: 10.1002/joc.656. URL `http://dx.doi.org/10.1002/joc.656`.

A. Robock, L. Luo, E. Wood, F. Wen, K. Mitchell, P. Houser, J. Schaake, D. Lohmann, B. Cosgrove, J. Sheffield, Q. Duan, R. Higgins, R. Pinker, J. Tarpley, J. Basara, and K. Crawford. Evaluation of the North American Land Data Assimilation System over the southern Great Plains during the warm season. *J. Geophy. Res.*, 109, 2004.

Royal Netherlands Meterological Institute. Effects of el niño on world weather. http://www.knmi.nl/research/global_−climate/enso/effects/, 2012.

F. Serinaldi, B. Bonaccorso, A. Cancelliere, and S. Grimaldi. Probabilistic characterization of drought properties through copulas. *PHYSICS AND CHEMISTRY OF THE EARTH*, 34(10-12):596–605, 2009.

J. Sheffield and E. F. Wood. Projected changes in drought occurrence under future global warming from multi-model, multi-scenario, IPCC AR4 simulations. *Climate Dynamics*, 31(1):79–105, JUL 2008. ISSN 0930-7575. doi: {10.1007/s00382-007-0340-z}.

J. Sheffield, E. F. Wood, and M. L. Roderick. Little change in global drought over the past 60 years. *Nature*, 491:435–438, November 2012.

J. Sheffield, G. Goteti, F. Wen, and E. Wood. A simulated soil moisture based drought analysis for the United States. *Journal Of Geophysical Research-Atmospheres*, 109(D24), 2004.

J. Shiau. Fitting drought duration and severity with two-dimensional copulas. *Water Resources Management*, 20(5):795–815, 2006.

S. Shukla and A. Wood. Use of a standardized runoff index for characterizing hydrologic drought. *Geophysical Research Letters*, 35(2), 2008. L02405.

S. Sorooshian, K.-L. Hsu, X. Gao, H. V. Gupta, B. Imam, and D. Braithwaite. Evaluation of persiann system satellite–based estimates of tropical rainfall. *Bulletin of the American Meteorological Society*, 81(9):2035–2046, 2013/01/07 2000. doi: 10.1175/1520-0477(2000)081<2035:EOPSSE>2.3.CO;2. URL `http://dx.doi.org/10.1175/1520-0477(2000)081<2035:EOPSSE>2.3.CO;2`.

S. Sorooshian, A. AghaKouchak, P. Arkin, J. Eylander, E. Foufoula-Georgiou, R. Harmon, J. M. H. Hendrickx, B. Imam, R. Kuligowski, B. Skahill, and G. Skofronick-Jackson. Advanced concepts on remote sensing of precipitation at multiple scales. *Bulletin of the American Meteorological Society*, 92(10):1353–1357, 2011a.

S. Sorooshian, A. AghaKouchak, P. Arkin, J. Eylander, E. Foufoula-Georgiou, R. Harmon, J. M. H. Hendrickx, B. Imam, R. Kuligowski, B. Skahill, and G. Skofronick-Jackson. Advancing the remote sensing of precipitation. *Bulletin of the American Meteorological Society*, 92(10):1271ñ1272, 2011b.

M. Svoboda, D. LeComte, M. Hayes, R. Heim, K. Gleason, J. Angel, B. Rippey, R. Tinker, M. Palecki, D. Stooksbury, D. Miskus, and S. Stephens. The drought monitor. *Bulletin of the American Meteorological Society*, 83(8):1181–1190, AUG 2002. ISSN 0003-0007.

K. E. Taylor, R. J. Stouffer, and G. A. Meehl. A summary of the cmip5 experiment design. Technical report, Lawrence Livermore National Laboratory, 2009.

K. E. Taylor, R. J. Stouffer, and G. A. Meehl. An Overview of CMIP5 and the Experiment Design. *Bulletin of the American Meteorological Society*, 93(4): 485–498, 2012. doi: {10.1175/BAMS-D-11-00094.1}.

H. C. S. Thom. A note on the gamma distribution. *Monthly Weather Review*, 86(4):117–122, 2013/01/06 1958. doi: 10.1175/1520-0493(1958)086<0117:ANOTGD>2.0.CO;2. URL http://dx.doi.org/10.1175/1520-0493(1958)086<0117:ANOTGD>2.0.CO;2.

K. Trenberth. Conceptual framework for changes of extremes of the hydrological cycle with climate change. *Climatic Change*, 42(1):327–339, MAY 1999. ISSN 0165-0009. doi: {10.1023/A:1005488920935}.

K. Trenberth. Climate variability and global warming. *Science*, 293(5527): 48–49, JUL 6 2001. ISSN 0036-8075. doi: {10.1126/science.293.5527.48}.

K. E. Trenberth. The definition of el niño. *Bulletin of the American Meteorological Society*, 78(12):2771–2777, 2013/01/06 1997. doi: 10.1175/1520-0477.

K. E. Trenberth, A. Dai, R. Rasmussen, and D. B. Parsons. The changing character of precipitation. *Bulletin of the American Meteorological Society*, pages 1205 – 1217, September 2003.

S. M. Vicente-Serrano, S. Beguería, J. Lorenzo-Lacruz, J. J. Camarero, J. I. López-Moreno, C. Azorin-Molina, J. Revuelto, E. Morán-Tejeda, and A. Sanchez-Lorenzo. Performance of drought indices for ecological, agricultural, and hydrological applications. *Earth Interactions*, 16(10):1–27, 2012/12/19 2012. doi: 10.1175/2012EI000434.1. URL http://dx.doi.org/10.1175/2012EI000434.1.

S. M. Vicente-Serrano, S. Begueria, and J. I. Lopez-Moreno. A Multiscalar Drought Index Sensitive to Global Warming: The Standardized Precipitation Evapotranspiration Index. *Journal of Climate*, 23(7):1696–1718, 2010.

J. P. Walker, G. R. Willgoose, and J. D. Kalma. In situ measurement of soil moisture: a comparison of techniques. *Journal of Hydrology*, 293(1–4):85–99, 6 2004. doi: http://dx.doi.org/10.1016/j.jhydrol.2004.01.008. URL http://www.sciencedirect.com/science/article/pii/S0022169404000393.

D. Wang, M. Hejazi, X. Cai, and A. J. Valocchi. Climate change impact on meteorological, agricultural, and hydrological drought in central Illinois. *Water Resources Research*, 47, SEP 27 2011. ISSN 0043-1397. doi: {10.1029/2010WR009845}.

S.-Y. Wang, R. R. Gillies, and T. Reichler. Multidecadal drought cycles in the great basin recorded by the great salt lake: Modulation from a transition-phase teleconnection. *Journal of Climate*, 25(5):1711–1721, 2013/01/06 2011. doi: 10.1175/2011JCLI4225.1. URL `http://dx.doi.org/10.1175/2011JCLI4225.1`.

B. Wardlow, M. Anderson, and J. Verdin. *Remote Sensing of Drought*. CRC Press, 2012.

WCRP. A wcrp white paper on drought predictability and prediction in a changing climate: Assessing current predictive knowledge and capabilities, user requirements and research priorities. Technical report, World Climate Research Programme, 2010.

M. Wehner. Methods of projecting future changes in extremes. In A. AghaKouchak, D. Easterling, K. Hsu, S. Schubert, and S. Sorooshian, editors, *Extremes in a Changing Climate: Detection, Analysis and Uncertainty*. Springer, 2012. DOI: 10.1007/978-94-007-4479-0 8.

N. Wells, S. Goddard, and M. J. Hayes. A Self-Calibrating Palmer Drought Severity Index. *Journal of Climate*, 17(12):2335–2351, 2013/01/06 2004. doi: 10.1175/1520-0442(2004)017<2335:ASPDSI>2.0.CO;2. URL `http://dx.doi.org/10.1175/1520-0442(2004)017<2335:ASPDSI>2.0.CO;2`.

D. Wilhite and M. Glantz. Understanding the drought phenomenon: The role of definitions. *Water Int.*, 10:111ñ120, 1985.

D. A. Wilhite. *Drought: a global assessment*, volume 2. Routledge HAzards and Disasters Series, 2000.

D. A. Wilhite, editor. *Drought and water crises: Science, technolog, and management issues.* Taylor and Francis Group, 2005.

D. Wilks. *Statistical Methods in the Atmospheric Sciences*. Academic Press, 1995.

WMO. Inter-regional workshop on indices and early warning systems for drought. Lincoln, nebraska, usa, 8-11 december 2009, World Meteorological Organization, 2009.

Wood E.F. and Sheffield J. Can we observe and assess whether the global hydrological cycle is "intensifying"? In *Abstract H12C-06 presented at 2012 Fall Meeting, AGU, San Francisco, Calif., 3-7 Dec.*, 2012.

J.-H. Yoon, K. Mo, and E. F. Wood. Dynamic-Model-Based Seasonal Prediction of Meteorological Drought over the Contiguous United States. *Journal of Hydrometeorology*, 13(2):463–482, 2012.

S. Yue, P. Pilon, and G. Cavadias. Power of the Mann–Kendall and Spearmanś rho tests for detecting monotonic trends in hydrological series. *Journal of Hydrology*, pages 254–271, 259.